nature neuroscience

ARTICLES

https://doi.org/10.1038/s41593-019-0366-7

Molecularly defined cortical astroglia subpopulation modulates neurons via secretion of Norrin

Sean J. Miller[1,2,3], Thomas Philips[1,2], Namho Kim[4,5], Raha Dastgheyb[6], Zhuoxun Chen[1,2], Yi-Chun Hsieh[1,2], J. Gavin Daigle[1,2], Malika Datta[7], Jeannie Chew[1,2], Svetlana Vidensky[1,2], Jacqueline T. Pham[1,2,3], Ethan G. Hughes[8], Michael B. Robinson[9,10], Rita Sattler[1,2], Raju Tomer[7], Jung Soo Suk[4,11], Dwight E. Bergles[8], Norman Haughey[6,12], Mikhail Pletnikov[12], Justin Hanes[4,5,11] and Jeffrey D. Rothstein[1,2,3,8]*

Despite expanding knowledge regarding the role of astroglia in regulating neuronal function, little is known about regional or functional subgroups of brain astroglia and how they may interact with neurons. We use an astroglia-specific promoter fragment in transgenic mice to identify an anatomically defined subset of adult gray matter astroglia. Using transcriptomic and histological analyses, we generate a combinatorial profile for the in vivo identification and characterization of this astroglia subpopulation. These astroglia are enriched in mouse cortical layer V; express distinct molecular markers, including Norrin and leucine-rich repeat-containing G-protein-coupled receptor 6 (LGR6), with corresponding layer-specific neuronal ligands; are found in the human cortex; and modulate neuronal activity. Astrocytic Norrin appears to regulate dendrites and spines; its loss, as occurring in Norrie disease, contributes to cortical dendritic spine loss. These studies provide evidence that human and rodent astroglia subtypes are regionally and functionally distinct, can regulate local neuronal dendrite and synaptic spine development, and contribute to disease.

Astroglia are the most abundant cell type in the CNS. They have essential roles in the development and homeostasis of the nervous system, maturation and maintenance of synapses, and regulation of neural transmission[1]. Disturbances of these essential roles may contribute to various CNS diseases, including amyotrophic lateral sclerosis (ALS)[1,2]. For more than 100 years, astroglia have been broadly defined into two morphologically described subgroups: protoplasmic astroglia, which are localized to gray matter; and fibrous astroglia, which are localized to white matter. However, recent years have witnessed a growing appreciation for potential astroglia diversity beyond simple morphology, with accumulating evidence suggesting the existence of functionally distinct astroglia subpopulations[1,3–7]. Current knowledge surrounding the regional specialization of astroglia populations comes in part from insight provided by the positional identity of astroglia in the developing spinal cord, where defined anatomical locations also define different astroglia subpopulations[4–6]. Each of these subpopulations displays a unique biological profile that allows the cell to maintain its physiological niche[8]. In disease, altered function in regional astroglia can contribute to neurotoxic events, such as impaired glutamate uptake by perisynaptic astroglia in the context of neurodegeneration[9]. However, very little is known about the molecular identities of different astroglia subgroups in the majority of CNS tissues and how these subgroups might regulate local neuronal function. This limited understanding of astroglia is due in part to the lack of RNA or protein markers to identify different subgroups in the adult CNS, making histological or functional studies of different populations nearly impossible. To begin to develop insight into possible astroglia subgroups, we explored the biology of an astroglia-specific targeted protein, the glutamate transporter excitatory amino acid transporter 2 (EAAT2), known to be focally altered in some disorders[10].

All astroglia normally express EAAT2, also known as glutamate transporter 1 (GLT1)[9]. Astroglial GLT1 is generally expressed uniformly throughout the CNS, although the levels of GLT1 are approximately tenfold higher in the hippocampus and cortex relative to the spinal cord[11]. Dramatic regional dysregulation of GLT1 expression has been observed in a variety of neurological and psychiatric disorders[9,12,13]. For example, GLT1 is downregulated in a subset of astroglia in the ventral spinal cord and layers of motor cortex in human ALS patients as well as in rodent models of ALS[2]. Although the biological basis of this focal dysregulation has

[1]Department of Neurology, Johns Hopkins University School of Medicine, Baltimore, MD, USA. [2]Brain Science Institute, Johns Hopkins University School of Medicine, Baltimore, MD, USA. [3]Cellular & Molecular Medicine, Johns Hopkins University School of Medicine, Baltimore, MD, USA. [4]The Center for Nanomedicine, Johns Hopkins University School of Medicine, Baltimore, MD, USA. [5]Department of Chemical and Biomolecular Engineering, Johns Hopkins University, Baltimore, MD, USA. [6]Department of Neurology, Richard T. Johnson Division of Neuroimmunology and Neurological Infections, Johns Hopkins University School of Medicine, Baltimore, MD, USA. [7]Department of Biological Sciences, Columbia University, New York, NY, USA. [8]Solomon H. Snyder Department of Neuroscience, Johns Hopkins University School of Medicine, Baltimore, MD, USA. [9]Children's Hospital of Philadelphia, University of Pennsylvania, Philadelphia, PA, USA. [10]Department of Ophthalmology, Johns Hopkins University School of Medicine, Baltimore, MD, USA. [11]Departments of Biomedical Engineering, Environmental and Health Sciences, Oncology, Neurosurgery, and Pharmacology and Molecular Sciences, Johns Hopkins University, Baltimore, MD, USA. [12]Department of Psychiatry, Johns Hopkins University School of Medicine, Baltimore, MD, USA. *e-mail: jrothstein@jhmi.edu

historically focused on how neurons may focally regulate GLT1 expression[14], in our attempts to define the regulation of GLT1 expression within astroglia specifically, we discovered a cortical layer- specific subpopulation with a unique molecular/protein signature that defines, in part, a functional role in regulating local neuronal dendrite and spine formation. We find that this novel astroglial pathway plays a fundamental role in the childhood neurological disorder, Norrie disease.

Results

Identification and validation of 8.3-astroglia: *Glt1* promoter reporter mouse lines. To examine *Glt1* regulation within astroglia, we created multiple mouse lines using DNA inserts that contained fragments of the *Glt1* promoter upstream of the *Glt1* transcriptional start site (TSS). Downstream of the *Gtl1* TSS, the insertion of a tdTomato reporter allowed us to visualize cell populations actively transcribing the transgenic constructs. The fragments of the *Glt1* promoter ranged from 2.5 kilobases (kb) to 8.3 kb upstream of the transcription start site (Fig. 1a and Supplementary Fig. 1A). These fragment sizes were chosen based on conserved genomic regions with high methylation between the mouse and human *Glt1* gene (human nomenclature, *EAAT2*) (Supplementary Fig. 1A). Multiple founder lines expressing a promoter fragment ≤ 7.9 kb showed tdTomato expression that was restricted to neurons (Fig. 1a and Supplementary Fig. 2A-B). Unexpectedly, founder lines with only a slightly larger insert size, 8.3 kb, showed tdTomato fluorescence limited to gray matter astroglia (Fig. 1a–c, Fig. 2a–c, and Supplementary Fig. 3B). Notably, a specific and reproducible subpopulation of gray matter astroglia expressed tdTomato in the cerebral cortex and several other regions unexplored in this study (Fig. 1b–d and Supplementary Fig. 3A; Supplementary Video 1). To compare this tdTomato-astroglia population (henceforth referred to as '8.3-astroglia') with all other gray matter cortical astroglia, we crossed 8.3-astroglia-labeled mice with a BAC-GLT1-enhanced green fluorescent protein (eGFP) mouse line (GLT1-eGFP), which labels all CNS astroglia with eGFP (Fig. 1a–d and Supplementary Fig. 3B)[11]. In the double transgenic mouse line (8.3-astroglia/GLT1-eGFP), all 8.3-astroglia were also eGFP$^+$, indicating that these cells are indeed astroglia expressing GLT1 (Fig. 2a–c and Supplementary Fig. 3B). In adult cortex gray matter, definable subsets of all eGFP astroglia were also tdTomato$^+$ (Fig. 1b,c and Supplementary Fig. 3B). Notably, 8.3-astroglia were completely absent from the hippocampus (Fig. 1d; Supplementary Movie 1).

The 8.3-astroglia consisted of approximately 28% of all cortical astroglia as evaluated by the number of 8.3-astroglia/GLT1-eGFP double-positive astroglia in the adult cortex (Fig. 2d and Supplementary Fig. 3C). Layer V of the cortex was preferentially enriched with 8.3-astroglia compared to all other cortical layers, whereas GLT1-eGFP single-positive astroglia were evenly distributed among the cortical layers as assessed by traditional two-dimensional as well as three-dimensional imaging approaches (Fig. 2e; Supplementary Video 1).

To verify that these observations were not due to an artifact of genomic integration, and to provide an alternative approach for studying this astroglia subset without the need for labeled transgenic mice, we introduced the 8.3 kb tdTomato plasmid in vivo in wild-type mice using nanoparticles. Nanoparticles have the advantage of accepting large molecular constructs and have excellent in vivo tissue distribution properties compared to adeno-associated viruses or lentiviruses[15,16]. Cytomegalovirus (CMV)-eGFP control and 8.3 kb tdTomato plasmids were packaged into separate nanoparticles that were approximately the size of nanometer-sized exosomes as visualized by transmission electron microscopy (Supplementary Fig. 3F-G). Following intracortical injection of CMV-eGFP control nanoparticles, eGFP fluorescence was distributed across the entire hemisphere and in all cell types (Supplementary Fig. 3D). However, after intracortical injection of the 8.3 kb tdTomato nanoparticles, tdTomato expression was limited to astroglia in the gray matter and specifically enriched in layers II/III and V, consistent with the 8.3-astroglia transgenic mouse (Fig. 2f and Supplementary Fig. 3E). These data support the hypothesis that the 8.3 kb sequence upstream of the *Glt1* TSS is used only by a subset of astroglia.

We next determined the stability of tdTomato fluorescence in this astroglia subset. Stable expression of tdTomato within a subset of astroglia throughout their life span, without the appearance of additional fluorescent signal from other cell populations, would support the use of tdTomato as a fluorescent marker to study the specific subset of cells using the 8.3 kb promoter fragment. To address this possibility, we performed longitudinal multiphoton imaging of the motor cortex (up to 500 µm deep) of 8.3-astroglia-labeled transgenic mice (Supplementary Video 2). We tracked individual 8.3-astroglia over a period of five weeks and saw no changes in fluorescence, nor did we observe the appearance of any additional tdTomato-expressing cells in the cortical regions studied (Fig. 2g; Supplementary Video 2). The cell-specific tdTomato fluorescence was first observed during developmental astrogenesis (P5) and remained stable throughout adulthood (not shown). Finally, we assessed the longitudinal expression of tdTomato in vitro using isolated 8.3-astroglia from adult mouse cortex (P60–P90), finding that tdTomato fluorescence continued for up to two weeks before cell passaging (Supplementary Fig. 4B-C). The continuous expression of tdTomato in 8.3-astroglia in vivo and in vitro supports the hypothesis that these cells represent a distinct subpopulation of astroglia and that this transgenic mouse model provides a tool to study this cell population in various contexts.

Molecular properties of 8.3-astroglia. We next assessed the unique molecular properties of the 8.3-astroglia by determining their transcriptomic profile. Adult mouse cortices ($n = 3$) were dissociated into single-cell suspensions and separated by fluorescence-activated cell sorting (FACS) to collect three distinct populations: GLT1-eGFP-only (gray matter astroglia); 8.3-astroglia (gray matter astroglia subset); and the negative-fluorescent cell population (all cells that were not gray matter astroglia) (Supplementary Fig. 4A)[17]. During FACS, we noted that tdTomato$^+$ astrocytes displayed varying levels of tdTomato fluorescence; however, we could only isolate the high expressers, which are continued to be referred to as 8.3-astroglia (Supplementary Fig. 4A). Based on microarray analysis of these populations, each group displayed a unique RNA transcriptome (Fig. 3a). As expected, the two astroglia populations were both enriched in well-established astroglia markers such as *Aldh1l1*, *Acsbg1*, and *Aqp4* (Fig. 3b)[18]. However, when comparing 8.3-astroglia to GLT1-eGFP astroglia and the reporter-negative cell population, the 8.3-astroglia in the cortex displayed consistent and profound enrichment in several candidate markers (Fig. 3c,d; Supplementary Table 1). Some of the highest expressing genes, which are also involved in neurological disorders, include *Kcnj10*, *Norrin*, *Olig2*, *Lgr6*, and *Fndc5* (Fig. 3c,d; Supplementary Table 2); their expression was validated using quantitative PCR (qPCR; Fig. 3d, data not shown).

Hypothesizing that these enriched proteins could provide clues into the unique biological properties of these adult astroglia subpopulations, and to allow us to create a combinatorial profile, we generated a list of markers enriched in single-positive GLT1-eGFP astroglia and double-positive astroglia populations and subjected these modified lists to software-based pathway analytics (Supplementary Tables 1, 3, and 4). We found that these astroglia populations were uniquely enriched in specific pathways, with enrichment of the Wnt/β-catenin signaling pathway in GLT1-eGFP astroglia and enrichment of the Sonic hedgehog pathway in 8.3-astroglia (Supplementary Fig. 4D). Both astroglia populations showed enrichment in pathways common to the function of all

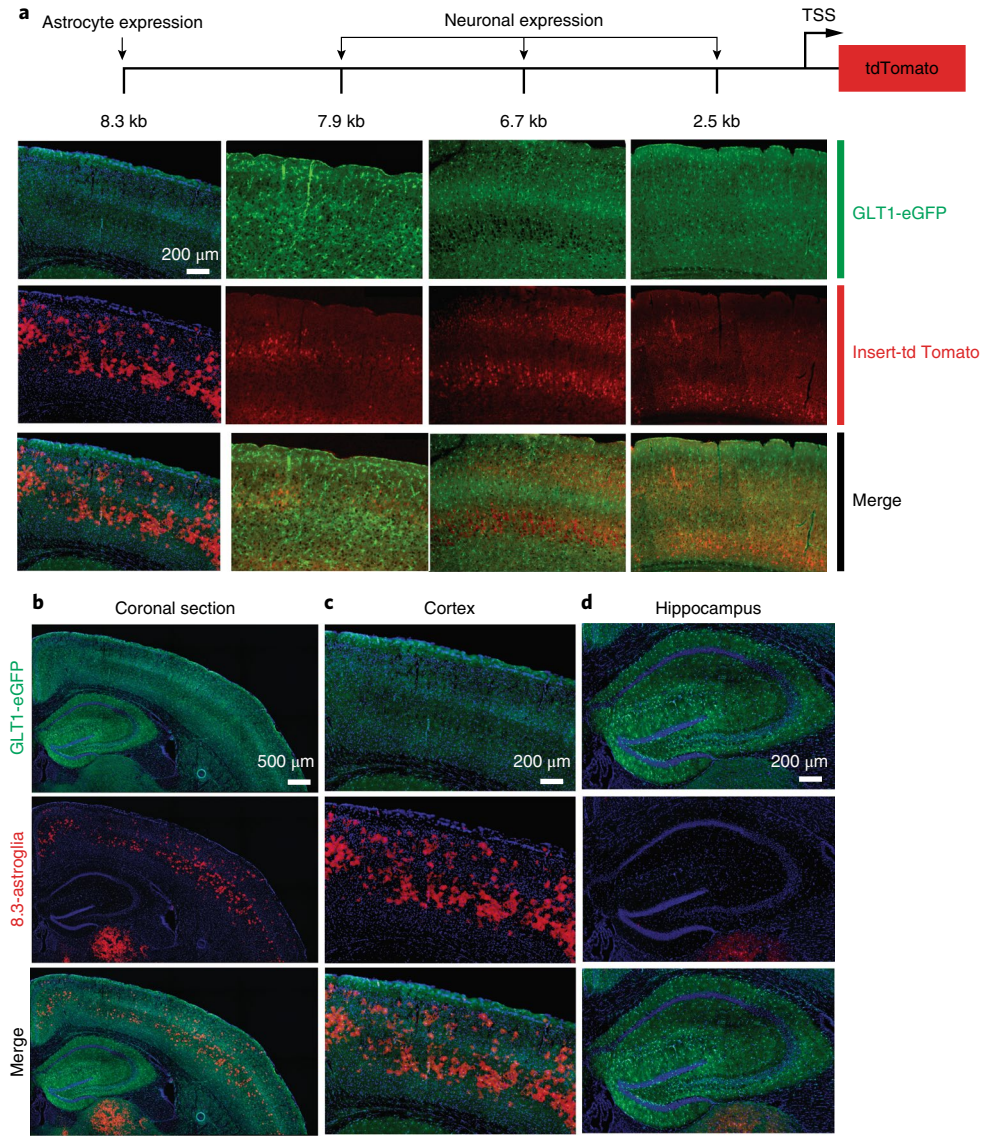

Fig. 1 | Generation of GLT1 promoter reporter mice employing increasing lengths of the DNA sequence upstream of the transcription start site. Promoter reporter mice were generated by employing different lengths of DNA sequences upstream of the TSS of GLT1 followed by tdTomato, leading to astroglia-specific tdTomato expression. **a**, Varying lengths of promoter-reporter fragments resulted in differential, cell-specific tdTomato expression. A fragment of 8.3 kb was required for astroglia-restricted tdTomato expression, whereas fragments ≤ 7.9 kb resulted in neuronal tdTomato expression and no astroglial expression in adults. **b**, Coronal section of the 8.3 kb tdTomato expression. **c**, Magnified image of motor cortex representing the overlap between 8.3 kb tdTomato and GLT1-eGFP astrocyte-specific expression. **d**, No 8.3 kb tdTomato expression was detected in the hippocampus. $N = 3$ different mice were imaged; 5 images per mouse were analyzed.

astroglia, such as pathways involved in fat synthesis (Supplementary Fig. 4D and Supplementary Tables 2 and 3)[19].

LGR6 and Norrin expression by 8.3-astroglia. We next sought to generate a panel of markers that could be used to uniquely identify 8.3-astroglia. Starting with candidates identified by our transcriptomic analyses, we assessed four genes that were highly enriched in 8.3-astroglia compared to both the GLT1-eGFP and negative-fluorescent cell populations: *Kcnj10*, *Lgr6*, *Olig2*, and *Norrin* (Fig. 3c,d; Supplementary Table 2). In agreement with our RNA analyses, the cortical distribution of KCNJ10 was enriched in similar regions as the 8.3-astroglia (Fig. 3e and Supplementary Fig. 5B-C). At higher magnification, 8.3-astroglia displayed a higher mean fluorescence intensity of KCNJ10 compared to GLT1-eGFP astroglia (Fig. 3e and Supplementary Fig. 5B-C). To visualize *Lgr6*-expressing cells, we generated a double transgenic mouse model by crossing LGR6-GFP-ires-CreERT2 mice with the 8.3-astroglia mice[20]. As expected, LGR6-eGFP localized to all 8.3-astroglia in the adult cortex of these double transgenic mice, with varying degrees of fluorescence (Fig. 3f). The LGR6-EGFP fluorescence was only noted in 8.3-astroglia and no other cells. We also detected nuclear OLIG2 expression in 8.3-astroglia, consistent with the microarray data (Supplementary Fig. 4E). We note that although OLIG2 is widely used to identify oligodendrocyte lineage cells in the CNS, it is also known to exist in some neuroprotective astroglia subpopulations[21,22]. In aggregate, the molecular identity and the unique CNS localization of the 8.3-astroglia are useful for elucidating the biological significance of this glial subgroup and allows the study of this subpopulation without the need of transgenic mice.

To determine whether this astroglia subpopulation is also present in the human cortex, we used LGR6 expression as a surrogate marker for the 8.3-astroglia population. Using immunohistochemistry

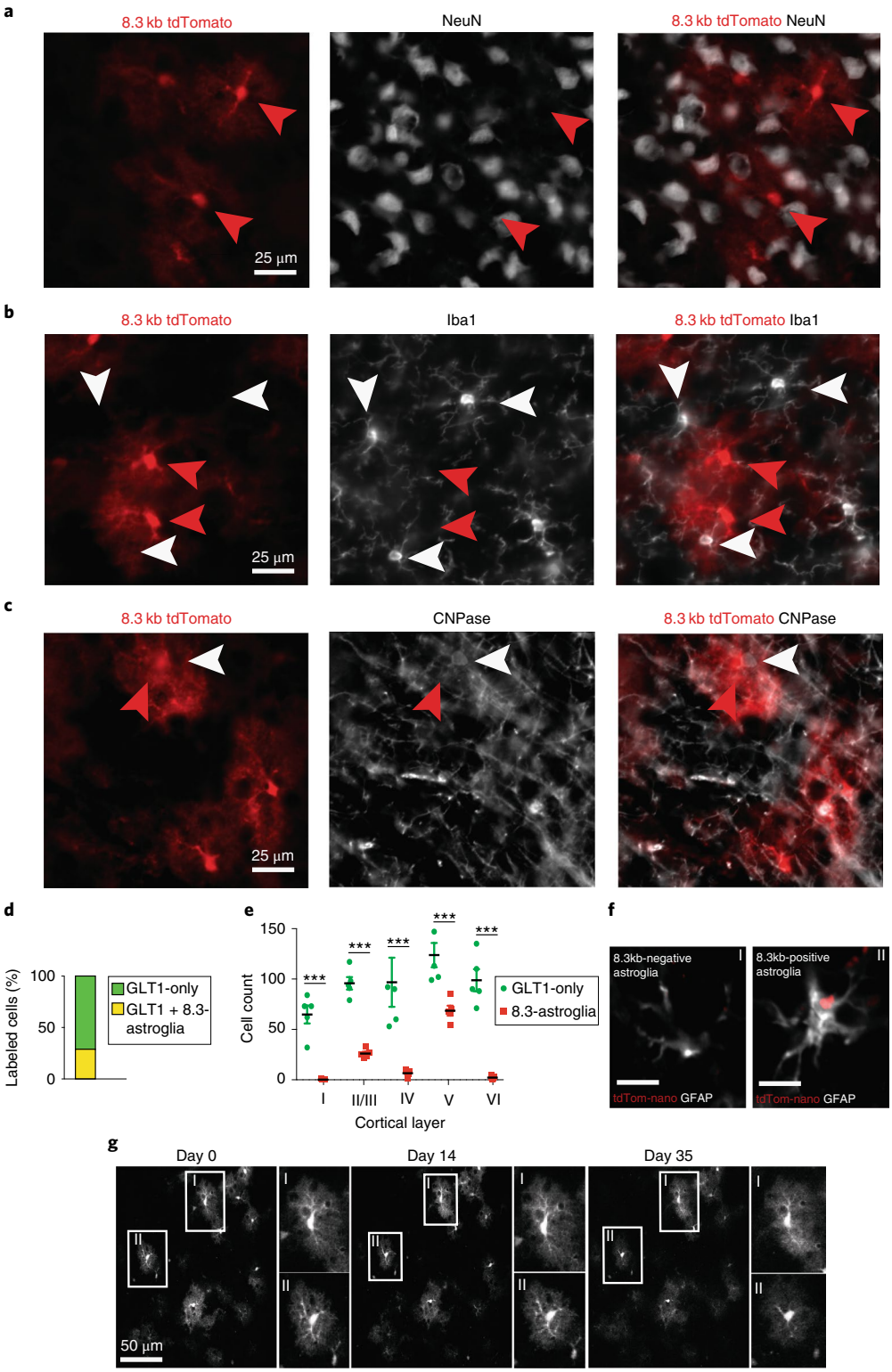

Fig. 2 | 8.3 kb tdTomato expression is static and limited to an astroglia subset in the cerebral motor cortex. a, 8.3 kb tdTomato does not colocalize with the neuronal marker NeuN. **b**, 8.3 kb tdTomato does not colocalize with the microglial marker Iba1. **c**, 8.3 kb tdTomato does not colocalize with myelin and the oligodendrocyte marker 2′,3′-cyclic-nucleotide 3′-phosphodiesterase (CNPase). **d**, 8.3-astroglia comprise about 25% of all gray matter astroglia in the motor cortex. **e**, 8.3-astroglia are heavily enriched in cortical layers II/III and V. GLT1-eGFP-only astroglia are equally distributed across all cortical layers. ***$P < 0.001$. **f**, 8.3 kb tdTomato nanoparticles are expressed by a subset of GFAP-positive astroglia enriched in layers II/III and V of the mouse motor cortex (scale bars, 15 µM). **g**, Cortical multiphoton in vivo imaging performed weekly for 5 weeks in adult mice tracking individual 8.3-astroglia ($N = 5$ mice, 100 cells). Astroglia cell counting was performed with sections imaged and subjected to validated automated cell counting of eGFP and tdTomato fluorescence cells. The statistics used to compare eGFP only to 8.3-astroglia per cortical layer included a two-way ANOVA with Tukey post hoc analysis. Error bars represent the s.e.m. For the nanoparticle injections, $n = 5$ mice were intracortically injected and analyzed. For all experiments, $n = 5$ mice were analyzed, with 3–5 images per mouse. The red arrowheads indicate the 8.3-astroglia and the white arrowheads indicate non-8.3-astroglia cells.

(IHC) and RNA in situ hybridization on postmortem adult human cortex tissue, we detected LGR6 expression in only a subset of astroglia in the human cortex, consistent with the results of our rodent studies (Fig. 3g,h and Supplementary Fig 5A). To validate the astroglia-specific expression of LGR6 in humans, we used IHC to visualize the astrocyte-specific marker ALDH1L1. LGR6 colocalized only with ALDH1L1$^+$ cells in the adult human cortex, providing further support that these cells are indeed a subset of human cortical astroglia (Fig. 3h and Supplementary Fig. 5A).

LGR6-positive astroglia subsets could also be reliably identified in vitro in both pure mouse primary cortical cultures and in human induced pluripotent stem cells (hiPSCs) differentiated into astroglia (Fig. 3i,j). We also observed a higher colocalization of KCNJ10 and LGR6 in hiPSC-derived astroglia, supporting the results of our combinatorial profile (not shown). Thus, these studies establish a well-defined and geographically organized astroglia subpopulation in the adult human and rodent cortex and provide reliable markers to study their involvement in normal and diseased adult CNS physiology.

Functional assessment of LGR6 in astroglia. We next aimed to determine the functional significance of our observation that the receptor LGR6 is consistently enriched and labels this astroglia subpopulation. In addition, we focused on LGR6 because it showed the highest enrichment in our RNA analytics and has been widely shown to be astroglia-specific in the CNS[23–25]. To address this question, we investigated the effects of adding its ligand, R-spondin (RSPO1). RSPO1 has been shown to be neuron-specific in the adult cortex, but little is known about the downstream consequences of its interaction with LGR6 in the CNS[8]. Consistent with published RNA in situ hybridization data, RSPO1 was highly enriched in 8.3-astroglia-dense areas in layer V (Fig. 4a and Supplementary Fig. 6A-D)[26]. Furthermore, we performed immunofluorescence for the neuronal marker, NeuN, followed by RNA fluorescence in situ hybridization (FISH) for RSPO1 and noted that RSPO1 colocalized only to NeuN-positive neurons, but only in a subset in the lower cortical layers (Supplementary Fig. 6A-D). This provides additional support that RSPO1 is neuron-specific in the adult motor cortex but that it is also limited to only a subset of neurons in cortical layer V.

Next, we wanted to explore the astroglia response to RSPO1 in vitro. Treatment of primary astroglia cultures with increasing doses of RSPO1 resulted in significant enrichment in the overall numbers of LGR6$^+$ astroglia compared to PBS-treated control cultures (Fig. 4b and Supplementary Fig. 7A-B). To determine whether this increase in LGR6$^+$ astroglia was due to proliferation, we stained astroglia with the proliferation marker Ki67, revealing a significant dose–response increase of Ki67-positive astroglia following RSPO1 treatment (Supplementary Fig. 7A). This increase in proliferation was due to an increase of LGR6$^+$ astroglia (Supplementary Fig. 7B). These in vitro findings suggest that in postnatal conditions, local neuronal release of RSPO1 could stimulate proliferation of astroglia, suggesting a specific interaction between an RSPO$^+$ neuron subpopulation and LGR6$^+$ 8.3-astroglia.

The stimulatory effect of LGR6 on the proliferation of 8.3-astroglia in vitro suggest that loss of LGR6 could decrease the population of 8.3-astroglia. Indeed, we observed a dramatic loss of 8.3-astroglia in vivo in the heterozygous 8.3-astroglia/LGR6-GFP-ires-CreERT2 mice, which have 50% lower expression of LGR6 compared to wild-type mice; this decrease further correlated with a minimal but significant loss of cortical thickness (Fig. 4c,d and Supplementary Fig. 7C). Since astroglia play a major role in neuronal synapse formation and elimination, we analyzed the overall density of spines on apical dendrites in layer V where 8.3-astroglia are highly enriched. We found a significant decrease in spine density in the heterozygous LGR6-eGFP/8.3-astroglia mouse model, correlating with the loss of 8.3-astroglia (Fig. 4e and Supplementary Fig. 8A-B).

Next, we sought to determine which factor(s) released by 8.3-astroglia could be responsible for the deficits in dendritic spine density, focusing on secreted proteins that were highly enriched in 8.3-astroglia as identified by our transcriptomic analyses. To test for the secretion of neuromodulating proteins, we stimulated LGR6$^+$ astroglia with RSPO1 and used enzyme-linked immunosorbent assay (ELISA) to detect candidate secreted proteins and determine which proteins increased with RSPO1 treatment. One highly abundant protein not enriched in the PBS control or LGR6 knockout primary astroglia was Norrin (norrin cystine knot growth factor NDP (*Ndp*)), a protein that is expressed in vivo by cortical astrocytes with strong colocalization with 8.3-astroglia in cortical layer V and has been shown to be astroglia-specific in the cortex (Fig. 4f–h)[23,27].

Norrin release by 8.3-astroglia regulates dendritic growth and spine formation. Norrin is known to be astroglia-specific in the adult cortex, where it binds to frizzled-4 and several other receptors such as LGR4 to activate the Wnt signaling pathway and thereby induce upregulation of neurotrophic growth factors, including brain-derived neurotrophic factor (BDNF)[28–30]. Patients with Norrin mutations develop Norrie disease, a CNS and ocular disease that also has strong cognitive and behavioral deficits including mental retardation, psychosis, and early-onset dementia in many but not all patients[31,32]. Some patients with Norrie disease have a deletion of exon 2, resulting in the possibility of two truncated proteins from exon 3. To evaluate the effects of increased Norrin on cortical neurons, we treated primary mouse cortical neurons with recombinant Norrin, compared to the PBS vehicle control and the two Norrin truncated proteins from exon 3 (referred to as 'truncated 1' and 'truncated 2') (Fig. 5a, Supplementary Fig. 9A-D, and Supplementary Fig. 10A-D). We found that treatment with both truncated proteins did not affect dendritic arborization or length;

Fig. 3 | Astroglial cell populations isolated from 8.3-astroglia mouse CNS and human cortex have unique transcriptomes, as validated with IHC and RNA in situ hybridization. a, The cortex microarray heatmap displays unique genes differentially expressed between all rodent astroglia (GLT1-eGFP), 8.3-astroglia and remaining non-labeled cells (negative). **b**, Microarray expression of astroglial markers highly expressed in both rodent astroglial populations. **c**, Selected markers highly enriched in 8.3-astroglia microarray data in the cortex. **d**, qPCR validation of candidate markers from the microarray analyses in the cortex of the three cell populations. **e**, KCNJ10 enhanced immunoreactivity in 8.3-astroglia compared to GLT1-eGFP astroglia in the mouse motor cortex. **f**, LGR6-GFP expression is restricted to 8.3-astroglia in the adult mouse cortex as evaluated in double transgenic LGR6-GFP-ires-CreERT2/8.3-astroglia mice. **g**, Analysis of *Lgr6* mRNA expression in the human motor cortex in a subset of cells; the arrowhead indicates RNA. DAPI, 4,6-diamidino-2-phenylindole. **h**, LGR6 protein in the human motor cortex colocalizes with GFAP and ALDH1L1 protein. **i**, A subset of cultured primary mouse cortical astroglia are LGR6$^+$. **j**, A subset of cultured and matured hiPSC astroglia are LGR6-immunoreactive. Three cell populations were isolated from the adult mouse whole cortex and subjected to FACS, microarray, and qPCR analyses from a total of three mice. For the histological sections, $n=5$ mice were imaged, with a minimum of 3–5 images per mouse; representative images are shown. Human postmortem tissue was evaluated from $n=3$ subjects without neurological disease, with at least 3–5 images taken per subject for both RNA in situ hybridization and IHC. For mouse immunocytochemistry, $n=5$ different cultures of mouse primary astroglia were generated and imaged at least 3–5 times per astroglial generation. For hiPSC astroglia, a minimum of three control hiPSC lines were generated. All images are representative of the total amount imaged. Two-sided Student's *t*-test of 8.3-astroglia versus negative cell population; the represented values show the mean and the error bars represent the s.e.m.

however, Norrin significantly affected dendritic arborization and increased dendritic length (Fig. 5b,c; data not shown). These findings show that the truncated Norrin protein translated in Norrie disease patients is inefficient at effecting neuronal dendrites.

Norrin has known effects on retinal biology, but its function in the cortex is unknown. To determine whether absence of Norrin would lead to neuronal deficits, we analyzed Norrin-null mice and quantified cortical neuron dendritic spine density. We found a significant loss of spines in cortical layer V in Norrin-null mice compared to their control littermates (Fig. 5d,e and Supplementary Fig. 8A,C).

Next, we wanted to evaluate the effects of in vivo Norrin treatment on cortical neuronal dendritic spine density. To address this, we created a genetic plasmid with the astroglia subset-specific 8.3 kb promoter followed by Norrin complementary DNA and packaged this plasmid into nanoparticles that were injected into the mouse motor cortex. Norrin secretion driven solely by the 8.3 kb promoter significantly increased dendritic spine density in the Norrin-null

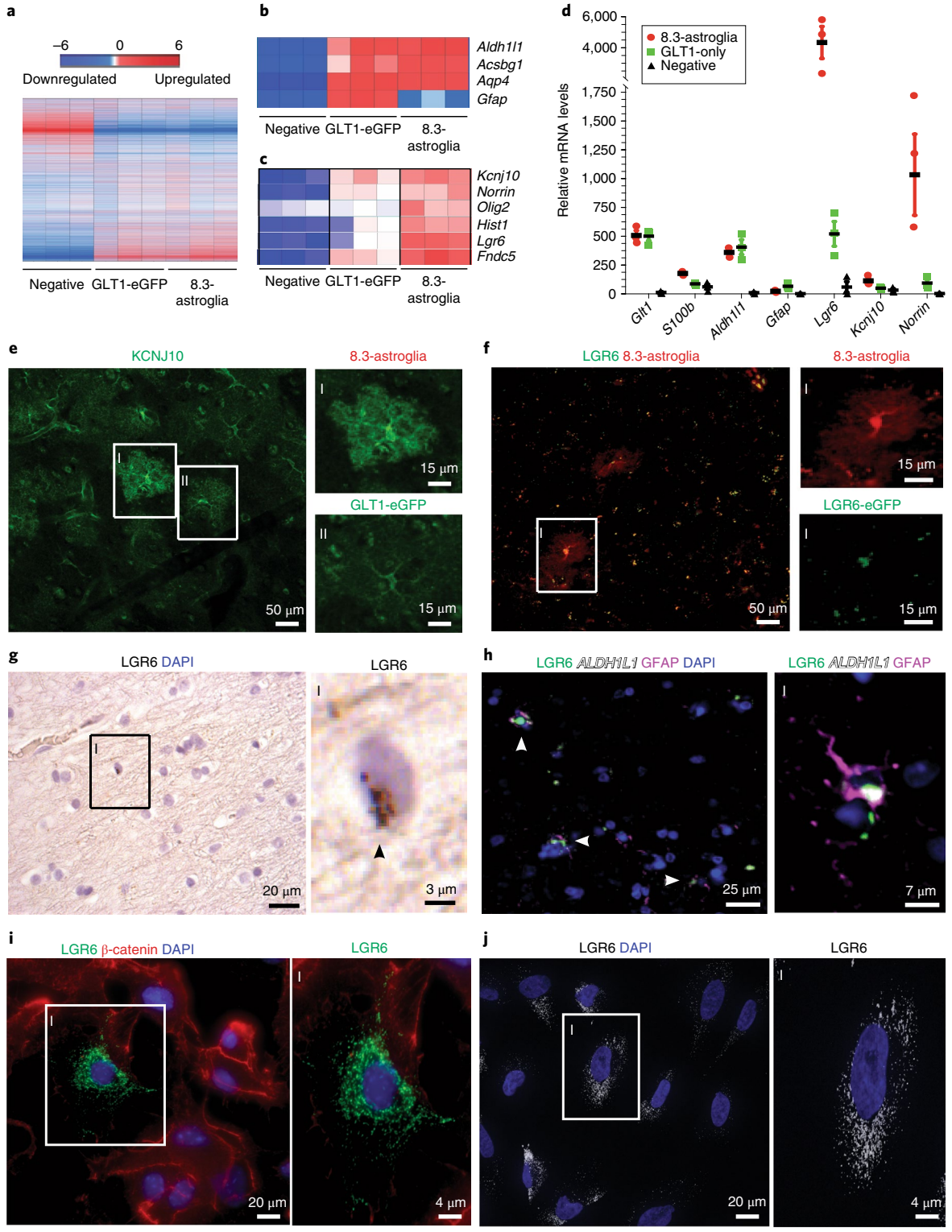

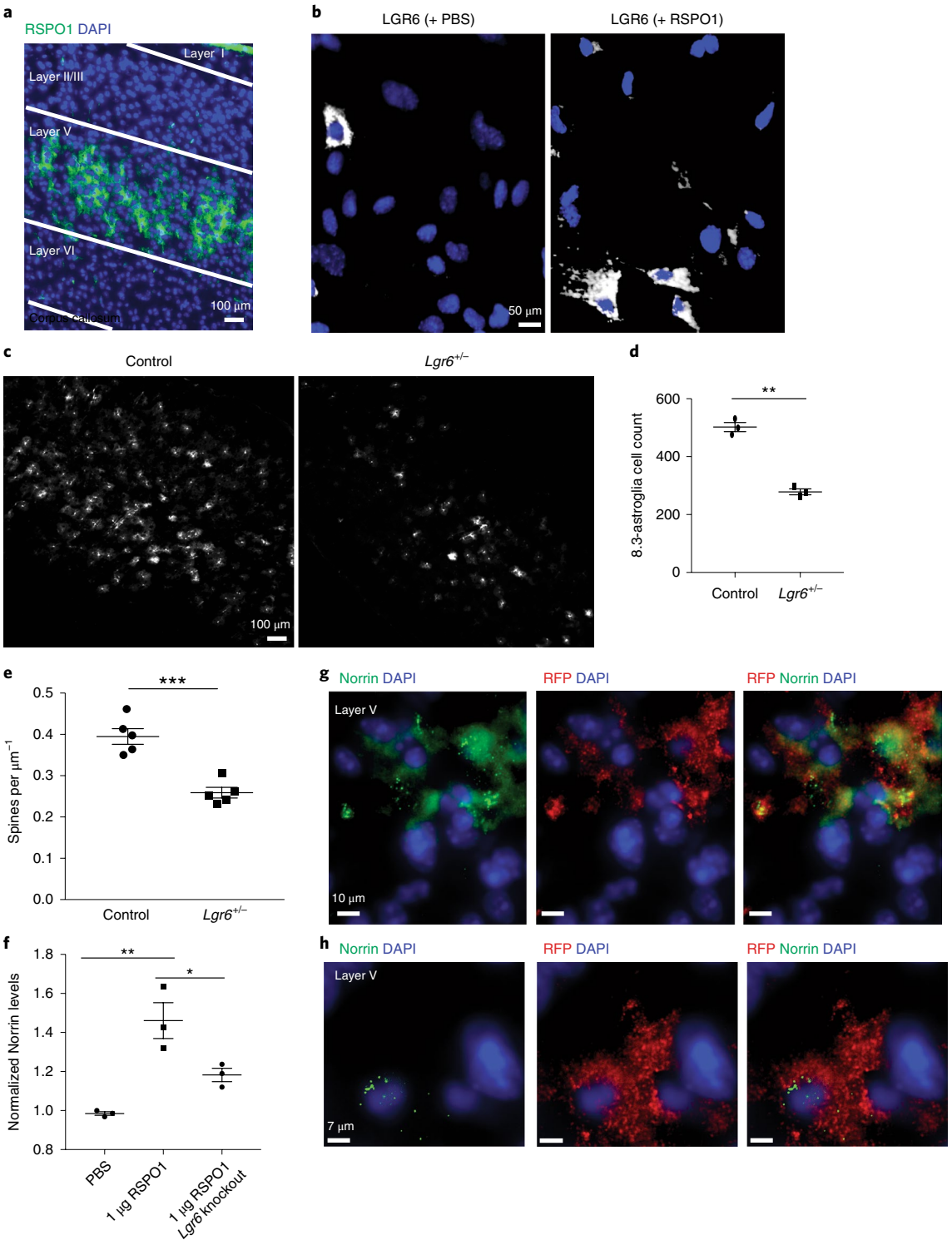

Fig. 4 | Functional and dysfunctional properties of astroglia subpopulation by examination of LGR6 pathways in the cerebral motor cortex. a, Neuron-specific RSPO1 immunoreactive localization is restricted to cortical layer V in the mouse motor cortex. **b**, RSPO1 treatment in vitro of primary mouse astroglia increases LGR6 immunoreactivity. **c**, *Lgr6* heterozygous mice display reduced numbers of 8.3-astroglia. **d**, *Lgr6* heterozygous mice display a significant reduction in the number of 8.3-astroglia; $P = 0.0003$. **e**, LGR6 alters the neurite properties; *Lgr6* heterozygous null mice have reduced spine density compared to control mice as assessed with the Golgi–Cox staining. **f**, The LGR6 receptor agonist RSPO1 affects astroglial Norrin. Norrin levels are increased following RSPO1 treatment on primary astroglia as assessed by ELISA. **g**, Norrin mRNA colocalizes with 8.3-astroglia in the mouse motor cortex. **h**, High magnification of colocalization of Norrin mRNA and tdTomato. $N = 5$ different mice with 3–5 coronal slices were imaged for IHC and RNA FISH. $N = 5$ mice were used for spine analysis with 5 neurons analyzed per mouse motor cortex. $N = 3$ different primary astroglia cultures were treated for 48 h with RSPO1 and repeated 3–5 times for ELISA analysis (control versus RSPO1: $P = 0.0025$; RSPO1 versus Lgr6 knockout: $P = 0.031$). Two-sided Student's *t*-test; values represent means and error bars represent s.e.m. $^{*}P < 0.05$, $^{**}P < 0.01$, $^{***}P < 0.001$.

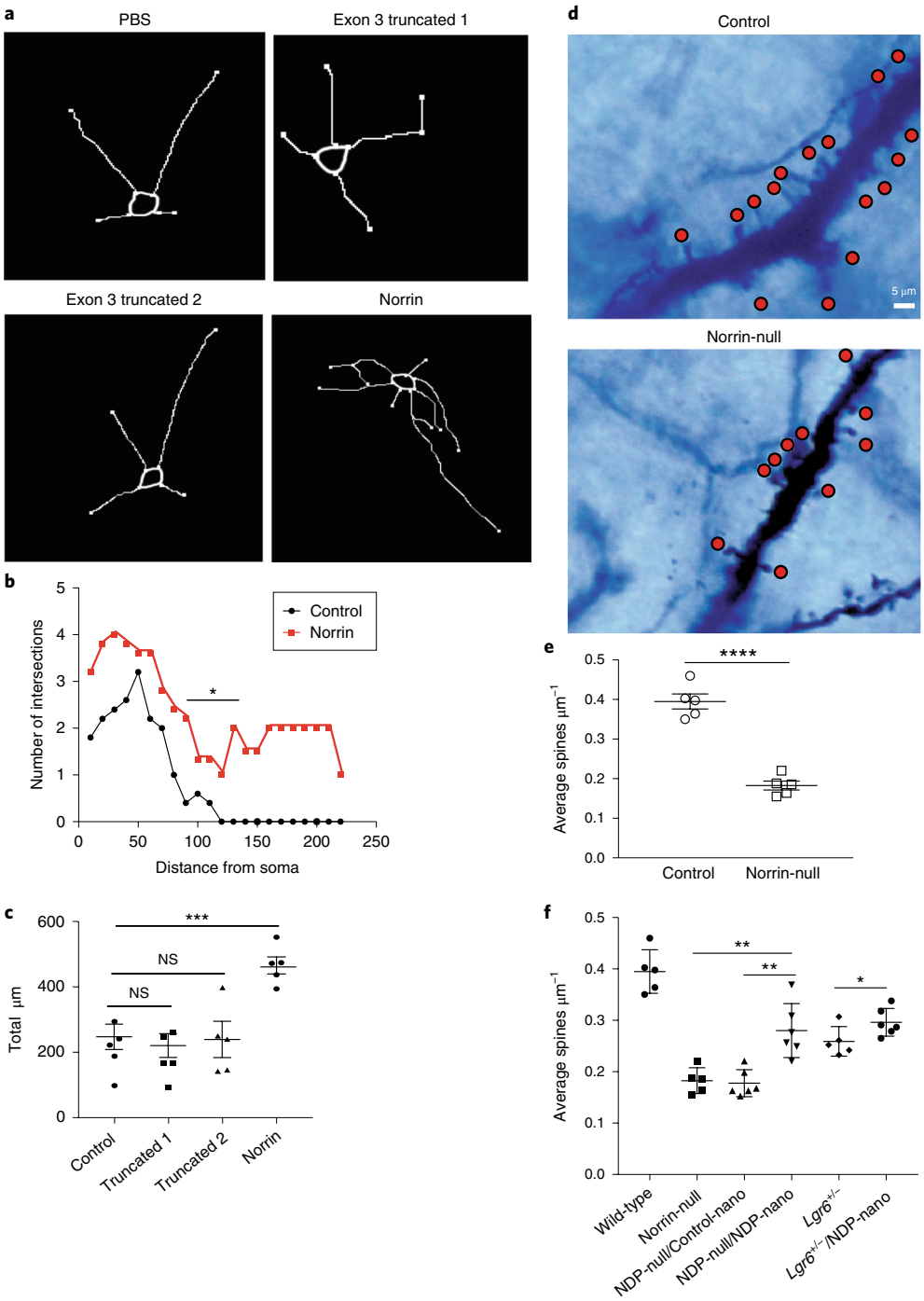

Fig. 5 | Norrin is a neuromodulating protein that affects cortical neuron dendritic morphology and spine density. a, Norrin-treated mouse cortical neurons show increased length and branching. **b**, Treatment with Norrin leads to a significant number of neurite changes, including intersections and neurite branchings as revealed by Scholl analytics. **c**, Neurite length is increased after Norrin treatment of cultured cortical mouse neurons. **d**, Loss of Norrin in vivo leads to a significant defect in cortical neuron spine density. Layer V cortical neurons were identified in adult Norrin-null mouse motor cortex and dendritic spines were examined after Golgi–Cox staining. **e**, Norrin-null mice have significantly reduced spine density compared to wild-type mice. **f**, Intracortical nanoparticle injections containing 8.3 kb Norrin significantly increase dendritic spine density in cortical layer V of the mouse motor cortex. For in vitro studies (**a**–**c**), recombinant Norrin and its truncated analogs were applied to 10 different isolations of cortical neurons ($n = 5$ mice) with a minimum of 20 neurons analyzed for each cohort for 48 h. For spine density analysis, $n = 5$ P60–P90 mice were analyzed using Golgi–Cox staining; 5–10 cortical neurons, located in the motor cortex cortical layer V, were counted and analyzed per genotype (representative images are shown). Two-sided Student's *t*-test comparing Norrin-treated versus control (**c**,**e**,**f**); $^{*}P < 0.05$, $^{**}P < 0.01$, $^{***}P < 0.001$, $^{****}P < 0.0001$. The values plotted represent the mean with the error bars representing the s.e.m.

and LGR6-eGFP-ires-CreERT2 mice compared to the CMV-eGFP control nanoparticle-injected Norrin-null and LGR6-eGFP-ires-CreERT2 mice (Fig. 5f). This provides evidence that Norrin produced solely by 8.3-astroglia is sufficient to restore the dendritic abnormalities and suggests a role for this astroglia-specific pathway in the regulation of neuronal spine and synaptic physiology.

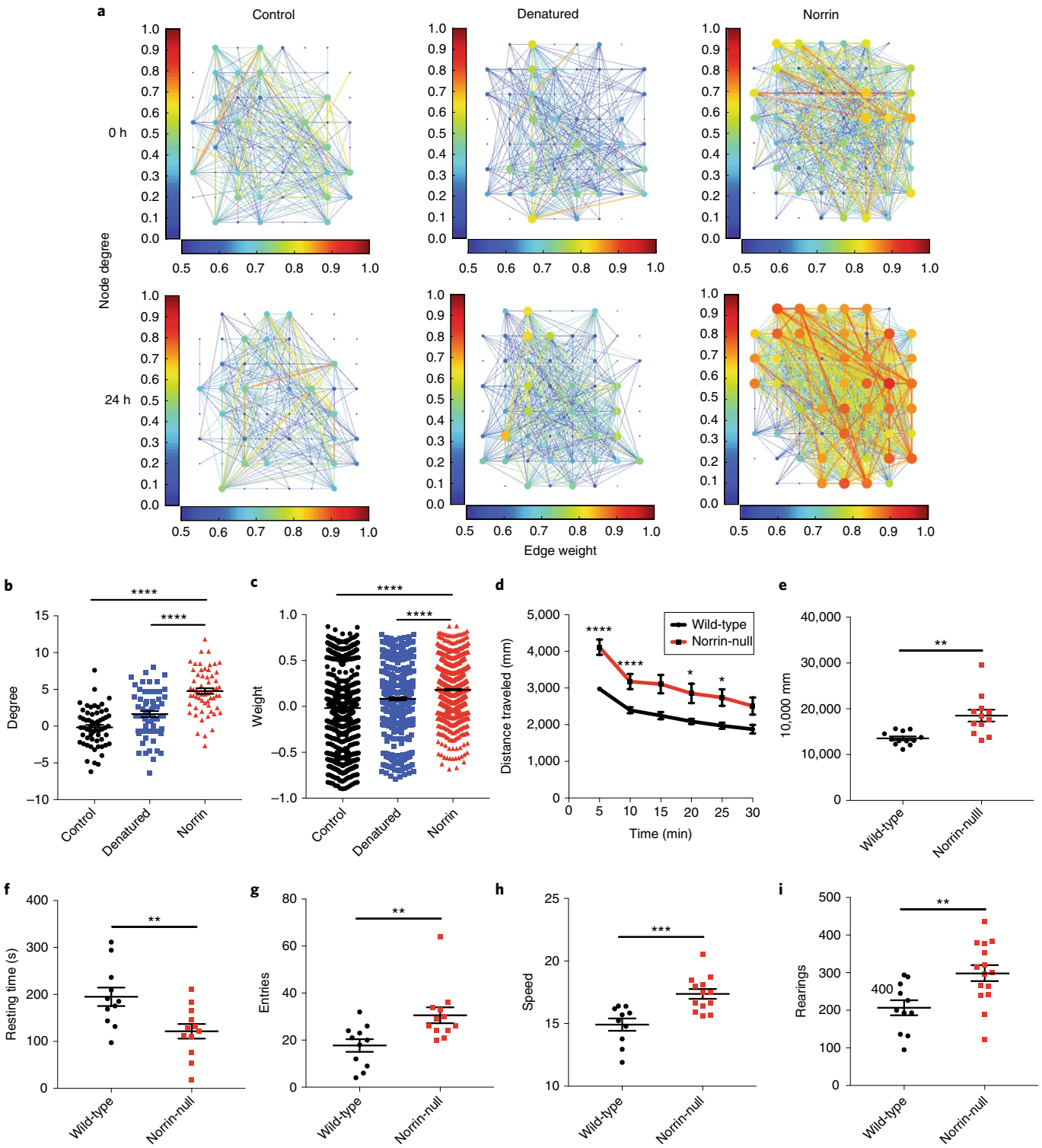

Fig. 6 | Norrin alters the electrophysiological properties of cortical neurons; Norrin-null mice display neurobehavioral abnormalities. a, Norrin treatment enhances cortical neuron connectivity and firing rate. **b**, Norrin treatment significantly increases the degree of neuronal firing. **c**, Norrin treatment significantly increases the weight of the neuronal firing strength. **d**, Norrin-null mice are significantly more hyperactive than their wild-type littermate controls. **e**, Total travel distance is significantly higher in Norrin-null mice compared to their wild-type littermate controls. **f**, Norrin-null mice have significantly decreased resting time compared to their wild-type littermate controls. **g**, Norrin-null mice have significantly more arm entries than their wild-type littermate controls. **h**, Norrin-null mice are significantly faster than their wild-type littermate controls. **i**, Norrin-null mice have significantly more rearings than their wild-type littermate controls. MEA analyses were performed three times at each time point, each with three different treatments. For the open field assay and Y-maze, $n = 15$–20 mice were used per genotype. Statistics include a two-way repeated-measures ANOVA and two-sided Student's *t*-test. **b**–**i**, $^{*}P < 0.05$, $^{**}P < 0.01$, $^{***}P < 0.001$, $^{****}P < 0.0001$. The values plotted represent the mean with the error bars representing the s.e.m.

Norrin treatment effects the electrophysiological properties of neurons. Next, we wanted to explore the effects of Norrin on the electrophysiology of cultured neurons. Using multielectrode array (MEA) plates with rat cortical neurons and astrocytes, we monitored basal activity before and 24 h after Norrin treatment (Fig. 6a and Supplementary Figs. 11A, 12A-F, and 13A; Supplementary Videos 3–5). Spike and burst rates were normalized to pretreatment activity to control for batch effects in baseline activity. There was a significant increase in the difference in both node degree and connection strength between electrodes, as well as a reorganization of spiking patterns wherein a greater percentage of detected spikes were organized into bursts (Fig. 6b,c and Supplementary Fig. 12A-F). These findings demonstrate that Norrin could function to organize and strengthen cortical neuronal connectivity.

Norrin-null mice display neurobehavioral abnormalities. Norrin-null mice displayed a pronounced loss of dendritic spines in layer V of the cortex and effected both electrophysiology and dendrites in vitro, so we sought to determine if they also displayed altered behavior. To test this hypothesis, we subjected the Norrin-null mice and their wild-type littermates to an array of behavioral assays. Surprisingly, in the open field assay, Norrin-null mice were significantly more hyperactive than their wild-type littermates, as shown by increased exploration and decreased resting time (Fig. 6d–f). In the Y-maze test, Norrin-null mice displayed increased combinations and arm entries, supportive of a hyperactive phenotype (Fig. 6g). Overall, the average speed of Norrin-null mice was significantly higher than the controls (Fig. 6h). When evaluating rearing, Norrin-null mice had significantly more rearing behaviors than their wild-type littermates (Fig. 6i). Furthermore, at this time period (P60–P90), these mice did not display abnormalities in several assays, such as the elevated platform maze, fear conditioning, and rotarod performance tests (data not shown). These findings further support that Norrin-null mice have neurobehavioral abnormalities, such as hyperactivity, which may be the result of their cortical phenotype.

Discussion

The majority of evidence for astroglia heterogeneity has arisen from developmental studies in the spinal cord or found as a pathological consequence in neurological disorders[6,9,33]. To date, there are few data that molecularly and/or physiologically define the presence of astroglia subsets in the adult nervous system that function to interact and/or regulate regional neuronal populations. Furthermore, no reliable tools exist to accurately and robustly identify these subpopulations in normal and disease states. With the generation of the 8.3-astroglia mouse line, we have discovered and are now able to easily study a specific astroglia subset in the cortex of adult mice. This astroglia subset, 8.3-astroglia, has distinct cortical patterns and molecular profiles compared to other gray matter astroglia; it can be robustly identified using unique markers such as OLIG2, NORRIN, KCNJ10, and LGR6 in rodent and human CNS, as well as in primary mouse and hiPSC astroglia cultures.

Our extensive profiling data have allowed us to generate a protein/RNA profile to molecularly identify 8.3-astroglia. LGR6 colocalizes with 8.3-astroglia in the mouse and human cortex, along with subsets of in vitro astroglia from rodents and in hiPSC-derived astroglia. LGR6 contributes to Wnt signaling, one of the pathways enriched in gray matter astroglia; its ligand, RSPO1, is specifically released by pyramidal neurons[8,20,34]. In the cortex of adult mice, we demonstrated that RSPO1 is restricted to a neuronal subset in layer V; these are areas highly enriched in LGR6$^+$ 8.3-astroglia. LGR6 and Norrin have both been shown to be highly enriched and limited to astroglia[23,25]. The correlation of RSPO1, LGR6, Norrin, and 8.3-astroglia cortical patterning strongly suggests that there may be a cross talk between neurons and astroglia, where extrinsic signaling, including the possible release of RSP01 from neuronal subtypes, could influence astroglia subtype-specific responses (Supplementary Fig. 14). In support of this model, RSPO1 is largely restricted to layer V of the cortex. Neurons influence astroglial physiology, for example, via astroglia expression of the glutamate transporter EAAT2[35]. Future studies should address the positional identity of specific astroglia and neuron populations where neuronal diversity may influence astroglia diversity and vice versa.

The unique anatomical localization of 8.3-astroglia and their enrichment in LGR6 and Norrin suggest that they may be involved in glial-based pathogenesis of Norrie disease. We document a selective loss of spine density in both the LGR6 heterozygous and Norrin-null mice in cortical layer V, corresponding to the location of 8.3-astroglia and Norrin expression. This is particularly interesting since some Norrie disease patients with genetic deletion of exon 2 of the *NDP* gene developed epilepsy. Epilepsy patients have been documented to have reduced spine density and altered dendritic arbor[36]. Unfortunately, it is not possible to analyze spine density in Norrie disease patients because there is no available postmortem brain tissue.

The effect of Norrin on cortical neuron dendrites is particularly interesting. We show that treating neurons with Norrin leads to increases in dendritic length and arborization. However, treatment with the two truncated Norrin proteins found in Norrie disease patients with deletion of exon 2 exhibited no effect on normal neuronal dendrites. Loss of spines is widespread in several disorders. In an ALS mouse model, there was a significant loss of spines in pyramidal layer V neurons in the motor cortex[37]. This is similar to the pathology in Alzheimer's disease, where dendritic spine loss is also involved[38]. In transcriptomic data of Alzheimer's disease mice, Norrin is significantly downregulated in astrocytes[39]. There is also an observed loss of Norrin levels in the hippocampus in Alzheimer's disease. Finally, reduced spine density is also observed in mental retardation (another documented phenotype in some Norrie disease patients)[38].

Norrin could serve as a potential therapeutic agent in neurological disorders with a spine density pathology. This is not the first report of astroglia regulating synapse maturation and receptors. Recently, the ability of astroglia to regulate the synaptic AMPA receptors and drive synapse maturation via chordin-like 1 was documented[40]. Now, we show that using the 8.3 kb-specific promoter to drive the expression of Norrin in the mouse cortex is sufficient to restore and improve cortical spine density. These data show that the sole release of Norrin strictly by 8.3-astroglia could serve as a therapeutic agent to modulate neuronal spines and synapses. Additionally, use of a ubiquitous promoter would hypothetically elevate Norrin levels even more and could lead to a more dramatic increase in spine density, altering dendritic arborization and length, and the electrophysiology of cortical neurons. In fact, the multielectrode array studies allowed us to test the effects of Norrin on the electrophysiological properties of neurons; Norrin treatment led to improved neuronal connectivity and strength supporting a possible role for this astroglia subpopulation in regulating neuronal connectivity and as a candidate therapy.

To assess the clinical phenotype of these mutant mice, we performed a wide array of behavioral assays on the Norrin-null mice. We found that Norrin-null mice displayed abnormal behavior in the open field and Y-maze tests. Overall, Norrin-null mice were hyperactive, which is similar to what has been shown in BDNF mutant mice; it has been shown that Norrin can drive the expression of BDNF and other neurotrophic proteins[29]. These neurobehavioral abnormalities might be expected in light of the cortical pathology of Norrin-null mice.

Lastly, the focal localization of the cortical layer of 8.3-astroglia is quite intriguing. Based on morphology, in the cortex different layers exhibit different populations of astroglia[41]. We have now shown that

the 8.3-astroglia subset is the dominant population of layer V astroglia. Different cortical layers exhibit different neuronal populations. Our findings provide further evidence that suggest a layer-specific cross talk between regional subsets of neurons and astroglia potentially indicating a localized neuron–glia functional specification. Future studies could explore this relationship, especially in disorders where a subset of cells is affected (that is, ALS motor neurons) as well as in paradigms of cortical synaptic plasticity.

Taken together, these findings expand the growing understanding of functional astroglial heterogeneity by uncovering and defining a unique subset of astroglia in the CNS. They have led to new tools to manipulate this astroglia subset in efforts to ultimately discover novel therapeutic avenues for neurological disorders affected by this and other astroglia subsets. This has also led to advances in the understanding Norrie disease, which we now define as also involving astroglia, and the contributions that astroglia may play in its pathophysiology. These studies have set a foundation to build on for understanding astroglial subsets, their powerful role in neuronal spine biology, and the unique neuron–glia pairing in normal and pathological states.

Online content

Any methods, additional references, Nature Research reporting summaries, source data, statements of data availability and associated accession codes are available at https://doi.org/10.1038/s41593-019-0366-7.

Received: 20 August 2018; Accepted: 15 February 2019;
Published online: 1 April 2019

References

1. Zhang, Y. & Barres, B. A. Astrocyte heterogeneity: an underappreciated topic in neurobiology. *Curr. Opin. Neurobiol.* **20**, 588–594 (2010).
2. Bruijn, L. I. et al. ALS-linked SOD1 mutant G85R mediates damage to astrocytes and promotes rapidly progressive disease with SOD1-containing inclusions. *Neuron* **18**, 327–338 (1997).
3. Molofsky, A. V. et al. Astrocyte-encoded positional cues maintain sensorimotor circuit integrity. *Nature* **509**, 189–194 (2014).
4. Tsai, H. H. et al. Regional astrocyte allocation regulates CNS synaptogenesis and repair. *Science* **337**, 358–362 (2012).
5. Oberheim, N. A., Goldman, S. A. & Nedergaard, M. Heterogeneity of astrocytic form and function. *Methods Mol. Biol.* **814**, 23–45 (2012).
6. Chaboub, L. S. & Deneen, B. Developmental origins of astrocyte heterogeneity: the final frontier of CNS development. *Dev. Neurosci.* **34**, 379–388 (2012).
7. Miller, S. J. Astrocyte heterogeneity in the adult central nervous system. *Front. Cell. Neurosci.* **12**, 401 (2018).
8. Zeisel, A. et al. Brain structure. Cell types in the mouse cortex and hippocampus revealed by single-cell RNA-seq. *Science* **347**, 1138–1142 (2015).
9. Rothstein, J. D., Van Kammen, M., Levey, A. I., Martin, L. J. & Kuncl, R. W. Selective loss of glial glutamate transporter GLT-1 in amyotrophic lateral sclerosis. *Ann. Neurol.* **38**, 73–84 (1995).
10. Rothstein, J. D. et al. Glutamate transporter subtypes: role in excitotoxicity and amyotrophic lateral sclerosis. *Ann. Neurol.* **36**, abstr. 282 (1994).
11. Regan, M. R. et al. Variations in promoter activity reveal a differential expression and physiology of glutamate transporters by glia in the developing and mature CNS. *J. Neurosci.* **27**, 6607–6619 (2007).
12. Tanaka, K. et al. Epilepsy and exacerbation of brain injury in mice lacking the glutamate transporter GLT-1. *Science* **276**, 1699–1702 (1997).
13. Higashimori, H. et al. Astroglial FMRP-dependent translational down-regulation of mGluR5 underlies glutamate transporter GLT1 dysregulation in the fragile X mouse. *Hum. Mol. Genet.* **22**, 2041–2054 (2013).
14. Swanson, R. A. et al. Neuronal regulation of glutamate transporter subtype expression in astrocytes. *J. Neurosci.* **17**, 932–940 (1997).
15. Ellis, B. L., Hirsch, M. L., Porter, S. N., Samulski, R. J. & Porteus, M. H. Zinc-finger nuclease-mediated gene correction using single AAV vector transduction and enhancement by Food and Drug Administration-approved drugs. *Gene Ther.* **20**, 35–42 (2013).
16. Parr-Brownlie, L. C. et al. Lentiviral vectors as tools to understand central nervous system biology in mammalian model organisms. *Front. Mol. Neurosci.* **8**, 14 (2015).
17. Foo, L. C. Purification of astrocytes from transgenic rodents by fluorescence-activated cell sorting. *Cold Spring Harb. Protoc.* **2013**, 551–560 (2013).
18. Cahoy, J. D. et al. A transcriptome database for astrocytes, neurons, and oligodendrocytes: a new resource for understanding brain development and function. *J. Neurosci.* **28**, 264–278 (2008).
19. Nieweg, K., Schaller, H. & Pfrieger, F. W. Marked differences in cholesterol synthesis between neurons and glial cells from postnatal rats. *J. Neurochem.* **109**, 125–134 (2009).
20. Snippert, H. J. et al. *Lgr6* marks stem cells in the hair follicle that generate all cell lineages of the skin. *Science* **327**, 1385–1389 (2010).
21. Jiang, P. et al. hESC-derived Olig2^{+} progenitors generate a subtype of astroglia with protective effects against ischaemic brain injury. *Nat. Commun.* **4**, 2196 (2013).
22. Tatsumi, K. et al. Olig2-lineage astrocytes: a distinct subtype of astrocytes that differs from GFAP astrocytes. *Front. Neuroanat.* **12**, 8 (2018).
23. Hrvatin, S. et al. Single-cell analysis of experience-dependent transcriptomic states in the mouse visual cortex. *Nat. Neurosci.* **21**, 120–129 (2018).
24. Schaum, N. et al. Transcriptomic characterization of 20 organs and tissues from mouse at single cell resolution creates a *Tabula Muris*. *Nature* **562**, 367–372 (2018).
25. Zhang, Y. et al. An RNA-sequencing transcriptome and splicing database of glia, neurons, and vascular cells of the cerebral cortex. *J. Neurosci.* **34**, 11929–11947 (2014).
26. Li, J. Y. et al. LGR4 and its ligands, R-spondin 1 and R-spondin 3, regulate food intake in the hypothalamus of male rats. *Endocrinology* **155**, 429–440 (2014).
27. Ye, X., Smallwood, P. & Nathans, J. Expression of the Norrie disease gene (*Ndp*) in developing and adult mouse eye, ear, and brain. *Gene Expr. Patterns* **11**, 151–155 (2011)./5/5/20
28. Braunger, B. M. & Tamm, E. R. The different functions of Norrin. *Adv. Exp. Med. Biol.* **723**, 679–683 (2012).
29. Seitz, R., Hackl, S., Seibuchner, T., Tamm, E. R. & Ohlmann, A. Norrin mediates neuroprotective effects on retinal ganglion cells via activation of the Wnt/β-catenin signaling pathway and the induction of neuroprotective growth factors in Muller cells. *J. Neurosci.* **30**, 5998–6010 (2010).
30. Deng, C. et alMulti-functional norrin is a ligand for the LGR4 receptor. *J. Cell Sci.* **126**, 2060–2068 (2013).
31. Ott, S., Patel, R. J., Appukuttan, B., Wang, X. & Stout, J. T. A novel mutation in the Norrie disease gene. *J. AAPOS* **4**, 125–126 (2000).
32. Warburg, M. Norrie's disease. *Birth Defects Orig. Artic. Ser.* **7**, 117–124 (1971).
33. Tong, X. et al. Astrocyte Kir4.1 ion channel deficits contribute to neuronal dysfunction in Huntington's disease model mice. *Nat. Neurosci.* **17**, 694–703 (2014).
34. Liao, X. H. & Nguyen, H. Epidermal expression of Lgr6 is dependent on nerve endings and Schwann cells. *Exp. Dermatol.* **23**, 195–198 (2014).
35. Yang, Y. et al. Presynaptic regulation of astroglial excitatory neurotransmitter transporter GLT1. *Neuron* **61**, 880–894 (2009).
36. Swann, J. W., Al-Noori, S., Jiang, M. & Lee, C. L. Spine loss and other dendritic abnormalities in epilepsy. *Hippocampus* **10**, 617–625 (2000).
37. Fogarty, M. J., Noakes, P. G. & Bellingham, M. C. Motor cortex layer V pyramidal neurons exhibit dendritic regression, spine loss, and increased synaptic excitation in the presymptomatic hSOD1^{G93A} mouse model of amyotrophic lateral sclerosis. *J. Neurosci.* **35**, 643–647 (2015).
38. Fiala, J. C. S. J., Spacek, J. & Harris, K. M. Dendritic spine pathology: cause or consequence of neurological disorders? *Brain Res. Brain Res. Rev.* **39**, 29–54 (2002).
39. Orre, M. et al. Isolation of glia from Alzheimer's mice reveals inflammation and dysfunction. *Neurobiol. Aging* **35**, 2746–2760 (2014).
40. Blanco-Suarez, E., Liu, T. F., Kopelevich, A. & Allen, N. J. Astrocyte-secreted chordin-like 1 drives synapse maturation and limits plasticity by increasing synaptic GluA2 AMPA receptors. *Neuron* **100**, 1116–1132.e13 (2018).
41. Lanjakornsiripan, D. et al. Layer-specific morphological and molecular differences in neocortical astrocytes and their dependence on neuronal layers. *Nat. Commun.* **9**, 1623 (2018).

Acknowledgements

We thank the Johns Hopkins Deep Sequencing and Microarray Core Facility and C. Conover Talbot Jr. for insight on microarray, and analyses using the Partek and Spotfire software suites, H. Zhang for assistance with FACS at the Johns Hopkins University School of Public Health FACS Center, the Johns Hopkins Medicine Microscopy Core for the use of the Zeiss LSM 700 laser scanning confocal microscope, J. Nathans for the Norrin mice, L. Ostrow for postmortem tissue, and members of the Rothstein laboratory for helpful discussions. This work was funded by grants from the National Science Foundation Graduate Fellowship Research Program (S.J.M.), grant no. R01NS092067 (J.D.R., M.B.R.), and NIH grant no. R01NS094239 (J.D.R.).

Author contributions

S.J.M. designed, performed, and analyzed the experiments, and wrote the manuscript. T.P. performed and E.G.H. assisted with the window surgeries and multiphoton imaging. J.G.D. and S.V. cultured and isolated the primary cortical neurons and maintained the mouse colonies. J.C. helped in Golgi imaging and interpretation; M.P. helped in

behavioral assay generation and interpretation. Z.C. and Y-C.H. assisted with tissue dissociation and transferred samples to the Johns Hopkins University FACS and Sequencing/Microarray cores. N.K. generated the nanoparticles and performed the transmission electron microscopy, which was overseen by J.S.S. and J.H. M.D. and R.T. performed the tissue clearing and CLARITY-optimized light-sheet microscopy imaging. J.T.P. assisted with maintenance and differentiation of hiPSC lines. R.D. performed the MEA experimentation, which was overseen by N.H. M.B.R., R.S., and D.E.B. contributed to data interpretation and manuscript review. J.D.R. oversaw project development, experimental design, data interpretation, data representation, and manuscript writing.

Competing interests

S.J.M. and J.D.R. have filed a patent on the use of Norrin. The remaining authors declare no competing interests.

Additional information

Supplementary information is available for this paper at https://doi.org/10.1038/s41593-019-0366-7.

Reprints and permissions information is available at www.nature.com/reprints.

Correspondence and requests for materials should be addressed to J.D.R.

Journal peer review information: Nature Neuroscience thanks Matthew Holt, Baljit Khakh, and other anonymous reviewer(s) for their contribution to the peer review of this work.

Methods

General procedures. Investigators were blinded to the behavioral analysis of genetic subgroups of mice and to all quantitative IHC staining of tissue and cultures. Randomization was not relevant to the experiments performed in this study. We compared specific control and test conditions through either treatment or genetic indicators.

Animal models. Wild-type (C57BL/6; The Jackson Laboratory), LGR6-GFP-ires-CreERT2 (The Jackson Laboratory), Norrin-null (gift from J. Nathans), BAC-GLT1-eGFP, 2.5 kb tdTomato, 6.7 kb tdTomato, 7.9 kb tdTomato, and 8.3 kb tdTomato mice were used for the in vivo experiments. GLT1/EAAT2 tdTomato transgenic mice were generated by inserting the tdTomato reporter downstream of a 2.5 kb, 6.7 kb, 7.9 kb, or 8.3 kb EAAT2/GLT1 promoter fragment as detailed in part previously[42]. Multiple founders were established following pronuclear injection at the transgenic core laboratory of Johns Hopkins University.

The care and treatment of animals were in accordance with the National Institutes of Health (NIH) Guide for the Care and Use of Laboratory Animals, the Guidelines for the Use of Animals in Neuroscience Research, and the Johns Hopkins University Institutional Animal Care and Use Committee. Mice were housed at standard temperature (21 °C) in a light-controlled environment with ad libitum access to food and water. BAC-GLT1-eGFP mice were crossed with 8.3 kb tdTomato mice to generate double transgenic mice; 8.3 kb tdTomato mice were also bred with LGR6-GFP-ires-CreERT2 mice. Littermates were used as controls and for comparisons between different astroglia populations.

Generation of GLT1/EAAT2 promoter tdTomato transgenic mice. *GLT1/EAAT2 (2.5 kb) tdTomato.* The fluorescence protein tdTomato was cloned into downstream of the human EAAT2 promoter sequence (2.5 kb). This DNA fragment was injected into a mouse pronucleus to produce the transgenic mouse. The promoter sequence was based on the following: chr11:35440759-35443219, 2,461 base pairs (bp).

GLT1/EAAT2 (6.7 kb) tdTomato. The fluorescence protein tdTomato was cloned into downstream of the human EAAT2 promoter sequence (6.7 kb). This DNA fragment was injected into a mouse pronucleus to produce the transgenic mouse. The promoter sequence was based on the following: chr11:35439159-35449110, 6,752 bp.

GLT1/EAAT2 (7.9 kb) tdTomato. The fluorescence protein tdTomato was cloned into downstream of the human EAAT2 promoter sequence (7.9 kb). This DNA fragment was injected into a mouse pronucleus to produce the transgenic mouse. The promoter sequence was based on the following: chr11:35439159-35448435, 7,677 bp.

GLT1/ EAAT2 (8.3 kb) tdTomato. The fluorescence protein tdTomato was cloned into downstream of the human EAAT2 promoter sequence (8.3 kb). This DNA fragment was injected into a mouse pronucleus to produce the transgenic mouse. The promoter sequence was based on the following: chr11:35440759-35449110, 8,352 bp.

Nanoparticle preparation and injection. Brain-penetrating DNA nanoparticles were formulated as previously reported[43]. Briefly, polyethylenimine (PEI) was dissolved in ultrapure water and pH was adjusted to 7.5. Methoxy-PEG-N-hydroxysuccinimide (mPEG-NHS, 5 kDa; Sigma-Aldrich) was conjugated to 25 kDa branched PEI (Sigma-Aldrich) to yield highly PEGylated PEI (PEG-PEI). The synthesis of PEG-PEI was confirmed by nuclear magnetic resonance. GFP-encoding plasmid DNA driven by CMV promoter (phosphorylated eGFP) was purchased from Clontech Laboratories. Brain-penetrating DNA nanoparticles were formulated by a dropwise addition of 10 volumes of DNA (phosphorylated eGFP or 8.3 kb tdTomato at 0.2 mg ml^{-1}) to 1 volume of swirling polymer solution. Polymer solution was prepared at a nitrogen to phosphate ratio, indicative of polymer to DNA ratio, of 6 and at a PEG-PEI to PEI molar ratio of 3. After 30 min of incubation at room temperature, the brain-penetrating DNA nanoparticles were washed with three volumes of ultrapure water and concentrated to 1 mg ml^{-1} using Amicon Ultra Centrifugal Filters (100,000 molecular weight cutoff; EMD Millipore) to remove free polymers. The DNA concentration in brain-penetrating DNA nanoparticles was determined using a NanoDrop 1000 spectrophotometer (Thermo Fisher Scientific).

Generation of Norrin truncated proteins. Recombinant proteins were generated and obtained from GenScript. The following amino acid sequences were used.

Truncated protein 1: MVLLARCEGHCSQASRSEPLVSFSTVLKQPFRSSCHCC RPQTSKLKALRLRCSGGMRLTATYRYILSCHCEECNSGPLLCVASGWDNCRGS STSQGKTGKKRVKAKKDATILPGLCIF;

truncated protein 2: MLRGHATHCHLPVHPLLSLRGMQFLRPAAVCGFWMGQL.

In vitro adult 8.3-astroglia dissociation and culture. Briefly, a gentleMACS Octo Dissociator (Miltenyi Biotec) was used with the adult CNS dissociation kit (magnetic-activated cell sorting; Miltenyi Biotec). Adult 8.3-astroglia/GLT1-eGFP mice (P60–P90, $n = 3$) were perfused with PBS and the cortex was dissected. Astroglia were isolated according to the manufacturer's protocol. Dissociated cells were cultured on Matrigel-coated flasks. Cells were imaged every other day for up to 14 d, before passaging, on an inverted Olympus scope.

HiPSC astroglia differentiation. Patient fibroblasts (Supplementary Table 5) were collected at Johns Hopkins Hospital with patient consent (institutional review board protocol: NA_00021979) as described[44]. In vitro hiPSC astroglia were cultured and differentiated as previously described[45]. Briefly, hiPSCs were converted into rosettes and then subjected to neural induction toward the neural progenitor cell fate via SMAD inhibition[46]. After differentiation into neural progenitor cells, treatment with fetal bovine serum was added to induce astrogenesis. Astroglia-differentiating neural progenitor cells were subjected to cell passaging once confluency reached 80–90%. All astroglia were analyzed at the mature state (12–13 weeks) and verified with appropriate astroglia markers as previously published[45]. Patient demographics are available in Supplementary Table 5. Cells were differentiated and imaged at age-matched time points.

Cell treatments. Primary mouse astroglia cultures were treated with 250 ng to 1 µg of mouse recombinant carrier-free RSPO1 (R&D Systems) for 72 h. For the cortical neuronal experiments, primary cortical neurons were isolated, matured for 7–10 d, and then treated with 600 ng to 2 ug of mouse recombinant carrier-free Norrin (R&D Systems) or truncated protein 1 or truncated protein 2 or 1× PBS or dickkopf-related protein 1 for 24 h.

FACS. The cortex, spinal cord, or cerebellum from BAC-GLT1-eGFP/8.3 kb tdTomato double transgenic reporter mice (age P60–P90, $n = 3$ male mice per experiment) were analyzed with FACS. Mice were anesthetized with an intraperitoneal injection of ketamine/xylazine. Brain tissue was immediately dissected and dissociated as previously described[17]. Single cells were then sorted using a MoFlo Multi-laser Sorter high-speed cell sorter (MoFlo XDP Cell Sorter) and gated based on eGFP and tdTomato fluorescence (Supplementary Fig. 4A).

Microarray. The microarray procedure and analyses were performed as previously described[46]. Briefly, total RNA was isolated from FACS-sorted populations using an RNA isolation kit (QIAGEN) and the concentration was determined by NanoDrop 2000/2000c Spectrophotometer (Thermo Fisher Scientific) and Bioanalyzer Micro 2 Scanner (Agilent). Only samples with an RNA integrity number > 5 were used. Total RNA was lineally amplified and labeled according to a NuGEN protocol. Sample labeling and hybridization with mouse exon 1.0 ST chips (Affymetrix) were performed at the Johns Hopkins University Deep Sequencing and Microarray Core according to the manufacturer's protocol. After hybridization, hybridization signals were acquired and normalized with the Partek Genomics Suite software (Partek). Differential gene expression between conditions was assessed by statistical linear model analysis using Partek, TIBCO Spotfire X, and Prism version 7 (GraphPad Software) software. The moderated *t*-statistic *P* values derived from the Partek analysis were further adjusted for multiple testing using the Benjamini–Hochberg method to control the false discovery rate. A false discovery rate cutoff of < 10% was used to obtain the list of differentially expressed genes. Tissue from at least three mice were used for each microarray analysis. All RNA array data is available online without restriction from the Gene Expression Omnibus.

Pathway analyses. Gene Ontology and pathway analyses were performed from data obtained from the Partek and Spotfire post-statistical analyses using the Ingenuity Pathway Analysis Genomics Suite software (QIAGEN) as previously described[46].

Histological analysis. *Brain IHC.* Mice were injected with a lethal dose of ketamine/xylazine and immediately perfused with 1× PBS followed by 4% paraformaldehyde (PFA). Post-perfusion, the brain, cerebellum, and spinal cord tissues were collected and cryoprotected in 30% sucrose. Tissue samples were prepared for cryostat sectioning and sectioned at a thickness of 20 µm. Sections were treated with blocking buffer (5% donkey serum and 0.1% Triton X-100 in PBS) for 60 min at room temperature. The following primary antibodies were used: GFP (1:100; Rockland); OLIG2 (1:250; EMD Millipore); glial fibrillary acidic protein (GFAP; 1:250; EMD Millipore); LGR6 (1:100; Abcam and R&D Systems); KCNJ10 (1:200; Alomone Labs); RSPO1 (1:100; Abcam); Norrin (1:100; Abcam); RFP (1:250; Abcam); and ALDH1L1 (1:100; Abcam). Secondary antibodies were: Alexa Fluor 647 donkey anti-rabbit (1:500; Abcam); Alexa Fluor 488 donkey anti-rabbit (1:500; Abcam); Alexa Fluor 488 donkey anti-mouse (1:500; Abcam); donkey anti-rabbit Cy3 (1:500; Abcam); and donkey anti-mouse Cy3 (1:500; Abcam). The use of the antibodies and their protein specificity was determined by each commercial vendor as provided on their websites or in their catalogs. Labeled cells were manually counted or overall fluorescence was calculated with the Zen Zeiss 2012 software or using spot detection in the Bitplane Imaris software version 8.3.1[47]. All images were captured with a Zeiss LSM 700 confocal microscope, Zeiss Axio Imager, or Zeiss LSM 800 confocal microscope. A minimum of three mice per group were used for each experiment at ages consistent with the microarray experiments (P60–P90).

Cell culture immunocytochemistry. Cells were stained as previously described[46]. Briefly, cells were grown until the appropriate time point or confluency followed by fixation in 4% PFA and 0.3% Triton X-100 permeabilization. Cells were then stained as described earlier.

Golgi–Cox staining. Tissue was processed according to the manufacturer's guidelines (FD Rapid GolgiStain Kit; FD Neurotechnologies).

CLARITY-optimized light-sheet microscopy. Samples in movie 1 ($n=2$) were imaged using CLARITY-optimized light-sheet microscopy by mounting in a quartz cuvette[48]. The objectives were immersed in a custom immersion liquid with a refractive index of 1.454 (Cargille Laboratories). For illumination, ×4/0.28 numerical aperture/29.5 mmWD (Olympus) objectives were used; a ×10/0.6 numerical aperture/8 mmWD (Olympus) objective was used for detection. The image volume was acquired with a 5 µm *z*-step size. Volume rendering was performed using 4×4-fold downsampled data with Amira v6.7 (FEI).

Tissue clearing. A passive CLARITY method was used for tissue clearing[48]. The hydrogel monomer solution recipe included 1% (wt/vol) acrylamide, 0.0125–0.05% (wt/vol) bis-acrylamide, 4% PFA, 1× PBS, deionized water, and 0.25% of the thermal initiator VA-044 (catalog no. NC0632395; Wako Chemicals). A transcardial perfusion was performed with hydrogel monomer and the brain was incubated overnight or 2 d at 4 °C with the hydrogel monomer solution. The tissue was then degassed to replace oxygen with nitrogen, followed by incubation at 37 °C for 3–4 h for hydrogel polymerization. Tissue was cleared in a 37 °C shaking incubator with a buffered clearing solution consisting of 4% (wt/vol) sodium dodecyl sulfate and 0.2 M boric acid (pH 8.5) with solution replacement every 1–2 d. After this step, the clearing solution was washed off with a 0.2 M boric acid buffer (pH 8.5)/0.1% Triton X-100. For imaging, tissues were mounted in 60% 2,2′-Thiodiethanol with 1× PBS[49].

RNA in situ hybridization. Human CNS tissue (Supplementary Table 5) was fixed in 4% PFA, cryoprotected in 30% sucrose, and samples were serially sectioned onto coverglass slides. RNA in situ hybridization was performed using the RNAscope duplex and chromogenic protocol as suggested by the manufacturer (Advanced Cell Diagnostics). Slides were imaged with a Zeiss Axio Imager brightfield camera. A minimum of three different brain samples were subjected to RNA in situ hybridization analyses. Hybridization probes were designed and purchased from RNAscope (Advanced Cell Diagnostics). Patient demographics are provided in Supplementary Table 5. Human tissue was obtained from Johns Hopkins and University of California, San Diego Target ALS Autopsy Bank. The use of human tissue and associated decedent demographic information was approved by the Johns Hopkins University institutional review board and ethics committee (HIPAA Form 5 exemption, application 11-02-10-01RD) and from the Target ALS Consortium.

In vivo imaging and surgical procedure. Adult (P60–P90, $n=5$ mice, 100 astroglia) mice were obtained from crosses of the BAC-GLT1-eGFP and 8.3 kb tdTomato mice. For repeated in vivo imaging, a cranial window was prepared as previously described[50]. In brief, mice were anesthetized with ketamine/xylazine and a craniotomy (3 mm diameter) was placed above the motor cortex. The craniotomy was covered with a permanent glass cover slip (4 mm diameter) and sealed with dental acrylic. For multiphoton imaging, mice were anesthetized with a mixture of oxygen and isoflurane. A metal head-bar was fixed over the craniotomy and placed into a head-bar holder for imaging. Mice were imaged weekly up to 500 µm below the dura using the Zeiss LSM 710 confocal microscope at the Johns Hopkins Neuroscience Imaging Core.

Mean intensity fluorescence analysis. 8.3-astroglia/GLT1-eGFP mice were stained with Kir4.1/Kcnj10 and analyzed with ImageJ (NIH). Briefly, the entire astroglia and processes were traced with the freehand tool to generate a region of interest. Next, the region of interest was measured for mean pixel density and recorded.

Cortical thickness calculation. The motor cortex from multiple mice ($n=5$) was imaged on the same reference slice; gross cortical thickness was measured by following the reference brain slice available from the Allen Brain Institute Reference Coronal Atlas.

Sholl analysis and dendritic length. Sholl analysis and dendritic length was determined with ImageJ as described previously[51].

Statistical analysis and sample size. Data was plotted in Prism version 7. One-way analysis of variance (ANOVA) with Bonferroni post hoc analysis, two-way repeated-measures ANOVA, and one-way or two-way Student's *t*-tests were used for statistical analyses where appropriate; see the figure legends for details ($^*P<0.05$, $^{**}P<0.01$, $^{***}P<0.001$). The s.e.m. was used for the errors bars ± mean. Data distribution was assumed to be normal, but this was not formally tested. No statistical methods were used to predetermine sample sizes, but our sample sizes are similar to those reported in previous publications.

Multielectrode array recordings. Multielectrode arrays were used to obtain extracellular voltage measurements and analyze functional connectivity. Primary neurons were cocultured with astrocytes at a density of 800 cells mm^{-2} on multichannel electrode array plates (60MEA200/30iR-Ti; MultiChannel Systems) coated with PEI (Sigma-Aldrich) and laminin (Sigma-Aldrich). Recordings were conducted beginning at DIV 14 using an MEA2100 system (MultiChannel Systems) on a stage heated to 37 °C. Voltage, spike, and burst measurements were obtained with the MC_RACK software (v4.6.2, MultiChannel Systems) and filtered using a second-order Butterworth filter with a 200 Hz cutoff frequency. Spikes were identified as instantaneous time points of voltages that exceed a threshold of at least 5 s.d. from baseline. Spike time stamps were exported using Multi Channel DataManager (v1.10.2.18155, MultiChannel Systems) and further analyzed using MEAnalyzer, where electrodes with high baseline noise (>60 µV) were excluded from the analysis. Bursts were identified as clusters of at least four spikes occurring within 100 ms of each other. MEAnalyzer was used to calculate spike rate, burst rate, burst length, the number of spikes in each burst, the percentage of spikes organized in bursts, and functional connectivity graphs based on spike rate. For the functional connectivity graphs, each electrode was considered a node; an 'edge' was created between two nodes if the connection strength between them exceeded a threshold of 0.5. Connection strength was defined as cross-correlation of binned spike rates (0.2 s bin widths) at a time lag of 0 that exceeded 0.5. The cross-correlation of electrode e_1 with electrode e_2 and at a time lag k for a recording of length T is as:[52]

$$\frac{1}{T}\sum_{t=1}^{T-k}(e_{1,t}-\overline{e}_1)(e_{2,t+k}-\overline{e}_2)\,;k=0,1,2\ldots$$

Once the connectivity graphs were created, several metrics were used to evaluate the network properties. Node degree is defined as the total number of connections for each node (represented as a percentage of the total nodes) and edge weight is the connection strength between two nodes[53].

Open field test. Spontaneous locomotion was analyzed using a VersaMax animal activity monitoring system with infrared beams (AccuScan Instruments). In brief, mice were placed in activity chambers for a total duration of 30 min. Horizontal and vertical activities, as well as the amount of time spent in the center or along the chamber walls, were automatically recorded.

Y-maze test. This test evaluates spatial working memory in a Y-maze. Mice were placed in one arm of the maze and spontaneous activity was recorded for 5 min. The number of entries in each of the three arms as well as the percentage of spontaneous alternations (mouse visiting all three arms without entering the same arm twice) was recorded.

Reporting Summary. Further information on research design is available in the Nature Research Reporting Summary linked to this article.

Data availability

The data supporting the findings of this study are available from the corresponding author upon reasonable request.

References

42. Yang, Y. et al. Molecular comparison of GLT1$^+$ and ALDH1L1$^+$ astrocytes in vivo in astroglial reporter mice. *Glia* **59**, 200–207 (2011).
43. Mastorakos, P. et al. Highly PEGylated DNA nanoparticles provide uniform and widespread gene transfer in the brain. *Adv. Healthc. Mater.* **4**, 1023–1033 (2015).
44. Zhang, K. et al. The *C9orf72* repeat expansion disrupts nucleocytoplasmic transport. *Nature* **525**, 56–61 (2015).
45. Li, Y. et al. A comprehensive library of familial human amyotrophic lateral sclerosis induced pluripotent stem cells. *PLoS One* **10**, e0118266 (2015).
46. Donnelly, C. J. et al. RNA toxicity from the ALS/FTD *C9ORF72* expansion is mitigated by antisense intervention. *Neuron* **80**, 415–428 (2013).
47. Miller, S. J. & Rothstein, J. D. Astroglia in thick tissue with super resolution and cellular reconstruction. *PLoS One* **11**, e0160391 (2016).
48. Tomer, R., Ye, L., Hsueh, B. & Deisseroth, K. Advanced CLARITY for rapid and high-resolution imaging of intact tissues. *Nat. Protoc.* **9**, 1682–1697 (2014).
49. Staudt, T., Lang, M. C., Medda, R., Engelhardt, J. & Hell, S. W. 2,2′-thiodiethanol: a new water soluble mounting medium for high resolution optical microscopy. *Microsc. Res. Tech.* **70**, 1–9 (2007).
50. Paukert, M. et al. Norepinephrine controls astroglial responsiveness to local circuit activity. *Neuron* **82**, 1263–1270 (2014).
51. Ferreira, T. A. et al.Neuronal morphometry directly from bitmap images. *Nat. Methods* **11**, 982–984 (2014).
52. Salinas, E. & Sejnowski, T. J. Correlated neuronal activity and the flow of neural information. *Nat. Rev. Neurosci.* **2**, 539–550 (2001).
53. Poli, D., Pastore, V. P. & Massobrio, P. Functional connectivity in in vitro neuronal assemblies. *Front. Neural Circuits* **9**, 57 (2015).

nature research

Corresponding author(s): Jeffrey D. Rothstein

Last updated by author(s): Feb 8, 2019

Reporting Summary

Nature Research wishes to improve the reproducibility of the work that we publish. This form provides structure for consistency and transparency in reporting. For further information on Nature Research policies, see Authors & Referees and the Editorial Policy Checklist.

Statistics

For all statistical analyses, confirm that the following items are present in the figure legend, table legend, main text, or Methods section.

n/a	Confirmed	
☐	☒	The exact sample size (*n*) for each experimental group/condition, given as a discrete number and unit of measurement
☐	☒	A statement on whether measurements were taken from distinct samples or whether the same sample was measured repeatedly
☐	☒	The statistical test(s) used AND whether they are one- or two-sided *Only common tests should be described solely by name; describe more complex techniques in the Methods section.*
☐	☒	A description of all covariates tested
☐	☒	A description of any assumptions or corrections, such as tests of normality and adjustment for multiple comparisons
☐	☒	A full description of the statistical parameters including central tendency (e.g. means) or other basic estimates (e.g. regression coefficient) AND variation (e.g. standard deviation) or associated estimates of uncertainty (e.g. confidence intervals)
☐	☒	For null hypothesis testing, the test statistic (e.g. *F*, *t*, *r*) with confidence intervals, effect sizes, degrees of freedom and *P* value noted *Give P values as exact values whenever suitable.*
☐	☒	For Bayesian analysis, information on the choice of priors and Markov chain Monte Carlo settings
☐	☒	For hierarchical and complex designs, identification of the appropriate level for tests and full reporting of outcomes
☐	☒	Estimates of effect sizes (e.g. Cohen's *d*, Pearson's *r*), indicating how they were calculated

Our web collection on statistics for biologists contains articles on many of the points above.

Software and code

Policy information about availability of computer code

Data collection	Prism 7, Microsoft Excel for Mac 2016
Data analysis	All software used was from publically available commercial computer software vendors in our lab or university used to collected data and image analysis:Prism 7, Microsoft Excel for Mac 2016,GenScript, Partek Genomics Suite, Tibco Spotfire, Ingenuity Pathway Analysis, Zen Zeiss 2012, Bitplane Imaris 8.3.1, ImageJ, MC_RACK, MDS DataManager, MEAnalyzer

For manuscripts utilizing custom algorithms or software that are central to the research but not yet described in published literature, software must be made available to editors/reviewers. We strongly encourage code deposition in a community repository (e.g. GitHub). See the Nature Research guidelines for submitting code & software for further information.

Data

Policy information about availability of data

All manuscripts must include a data availability statement. This statement should provide the following information, where applicable:

- Accession codes, unique identifiers, or web links for publicly available datasets
- A list of figures that have associated raw data
- A description of any restrictions on data availability

All microarray data will be uploaded to GEO for readers to access. Otherwise, all information has been stated in the manuscript.

Field-specific reporting

Please select the one below that is the best fit for your research. If you are not sure, read the appropriate sections before making your selection.

☒ Life sciences ☐ Behavioural & social sciences ☐ Ecological, evolutionary & environmental sciences

For a reference copy of the document with all sections, see nature.com/documents/nr-reporting-summary-flat.pdf

Life sciences study design

All studies must disclose on these points even when the disclosure is negative.

Sample size	samples sizes were chosen based on previous expertise, knowledge from past experiments and statistical considerations using similar model systems (neuron iPS cultures, mouse studies) and current accepted standards based on literature review. No statistic analysis was used to predetermine sample size. Sample sizes were chosen to be similar or exceed those reported in the previous literatures in the field. Each experiment was repeated 3-6 times, and the statistical analysis demonstrates that our sample sizes revealed significant differences between groups.
Data exclusions	No data were excluded from the study
Replication	All experiments were done with a minimum number of replicates based on previous expertise in statistical analyses of similar experimental datasets. Samples sizes were chosen based on previous expertise and knowledge from past experiments using similar rodent cultures, human CNS tissue, mouse in vivo studies and iPSC-derived systems and current accepted standards based on literature review. The findings in this study were collected from multiple independent experiments, and were reliably reproduced.
Randomization	Not relevant to this study. When appropriate, animals were randomly chosen for analytics form each genetic subgroup
Blinding	Investigators were blinded for behavioral analysis of genetic subgroups of mice and for all quantitative IHC staining of tissue and cultures.

Reporting for specific materials, systems and methods

We require information from authors about some types of materials, experimental systems and methods used in many studies. Here, indicate whether each material, system or method listed is relevant to your study. If you are not sure if a list item applies to your research, read the appropriate section before selecting a response.

Materials & experimental systems

n/a	Involved in the study
☐	☒ Antibodies
☐	☒ Eukaryotic cell lines
☒	☐ Palaeontology
☐	☒ Animals and other organisms
☐	☒ Human research participants
☒	☐ Clinical data

Methods

n/a	Involved in the study
☒	☐ ChIP-seq
☐	☒ Flow cytometry
☒	☐ MRI-based neuroimaging

Antibodies

Antibodies used

The following primary antibodies were used: (NEED CATALOG numbers)
GFP (Rockland), #600-401-215L; 600-401-215S
OLIG2 (Millipore), #AV31464
GFAP (Millipore), SAB2500462, MAB360, ab5320
GFAP (Abcam), ab53554, ab5541
LGR6 (Abcam, R&D Systems), ab240030
KCNJ10 (Alomone Labs), APC-035-AG
KCNj10 (Abcam), ab240876
RSPO1 (Abcam), ab106556; ab231125
Norrin (Abcam), ab185175, ab90690
ALDH1L1 (Abcam). ab87117, ab 56777
RFP (Abcam), ab62341

Secondary antibodies were all tested to be specific for the species identified.
donkey anti-rabbit Alexa Fluor 647 (Abcam), ab150073, ab175651
donkey anti-mouse Alexa Fluor 647 (Abcam), ab150107
donkey anti-rabbit 488 (Abcam), ab150061
donkey anti-mouse 488 (Abcam), ab150105

donkey anti-rabbit Cy3 (Jackson,Abcam), 711-165-152
donkey anti-mouse Cy3 (Jackson,Abcam), 715-005-150

Validation

The use of the antibodies and their protein specificity was determined by each commercial vender as provided by their websites:
GFP (Rockland): ELISA, WB, IHC, IF, FC
OLIG2 (Millipore), IHC,WB
GFAP (Millipore), ELISA,IHC,WB
LGR6 (Abcam, R&D Systems), flow, ICC, IHC, WB
KCNJ10 (Alomone Labs), IHC,ICC,WB
KCNJ10 (Alomone Labs), ICC, WB
RSPO1 (Abcam), IHC, WB
Norrin (Abcam), IHC, WB
ALDH1L1 (Abcam), ICC,IHC, WB

Secondary antibodies were all tested to be specific for the species identified.
donkey anti-rabbit Alexa Fluor 647 (Abcam), ELISA, flow, ICC,IHC
donkey anti-mouse Alexa Fluor 647 (Abcam),IHC, flow, ICC, ELISA
donkey anti-rabbit 488 (Abcam), ELISA, flow, IHC, ICC
donkey anti-mouse 488 (Abcam), ELISA, flow, IHC, ICC
donkey anti-rabbit Cy3 (Jackson,Abcam), IHC
donkey anti-mouse Cy3 (Jackson, Abcam).

Eukaryotic cell lines

Policy information about cell lines

Cell line source(s)

Primary mouse cortical neurons and astrocytes and primary rat cortical neurons were dissected and obtained based on the methods stated in the manuscript.

Authentication

Authentication was performed by validating with known pan-markers for the respective cell lines.

Mycoplasma contamination

All cell lines tested negative for mycoplasma contamination.

Commonly misidentified lines
(See ICLAC register)

No commonly misidentified cell lines were used.

Animals and other organisms

Policy information about studies involving animals; ARRIVE guidelines recommended for reporting animal research

Laboratory animals

Wild type (C57/BL6), LGR6-GFP-ires-CreERT2 (Jackson Laboratory), Norrin-null (gift from Jeremy Nathans), BAC-GLT1-eGFP, 2.5 kb-tdTomato, 6.7 kb-tdTomato, 7.9 kb-tdTomato, and 8.3 kb-tdTomato mice were used for in vivo experiments. GLT1/EAAT2-tdTomato transgenic mouse were generated by inserting the tdTomato reporter downstream of a 2.5kb, 6.7kb, 7.9 kb or 8.3kb EAAT2/GLT1 promoter fragment as detailed in part previously. Multiple founders were established following pronuclear injection at the transgenic core laboratory of Johns Hopkins University.
Mice were housed at standard temperature (21°C) in a light-controlled environment with ad libitum access to food and water. BAC-GLT1-eGFP mice were crossed with 8.3 kb-tdTomato mice to generate double transgenic mice. 8.3 kb-tdTomato mice were also bred with LGR6-GFP-ires-CreERT2 mice. Littermates were used as controls and for comparisons between different astroglia populations.

Wild animals

Please state that the study did not involve wild animals.

Field-collected samples

Please state that the study did not involve field collected samples.

Ethics oversight

The care and treatment of animals were in accordance with the NIH Guide for the Care and Use of Laboratory Animals, the Guidelines for the Use of Animals in Neuroscience Research, and the Johns Hopkins University IACUC.

Note that full information on the approval of the study protocol must also be provided in the manuscript.

Human research participants

Policy information about studies involving human research participants

Population characteristics

Human control CNS tissues were available from the Johns Hopkins Autopsy Tissue Bank maintained in our lab and the Target ALS postmortem core. For Target ALS specimens, a web-based searchable database of the postmortem tissue inventory provides estimates of fixed and frozen postmortem tissues available that meet basic demographic criteria.
Induced Pluripotent stem cell lines (iPS) were generated in our lab, under HIH-NIDNS supervision. These line were deposited in the NIH-NINDS cell repository and are publicly available thru NIH. Additional iPS cell lines are available thru the Neurolinc iPS cell consortium and obtained via the Cedars Sinai cell repository (https://www.cedars-sinai.edu/Research/Research-Cores/Induced-Pluripotent-Stem-Cell-Core-/)

Recruitment

Eligible patients and/or family members are recruited from our ALS clinic for voluntary participation in autopsy donations.

Ethics oversight	All autopsied and tissue collections are Johns Hopkins IRB approved with Johns Hopkins ethics oversight. All patient information is HIPPA complient.

Note that full information on the approval of the study protocol must also be provided in the manuscript.

Flow Cytometry

Plots

Confirm that:

☒ The axis labels state the marker and fluorochrome used (e.g. CD4-FITC).

☒ The axis scales are clearly visible. Include numbers along axes only for bottom left plot of group (a 'group' is an analysis of identical markers).

☒ All plots are contour plots with outliers or pseudocolor plots.

☒ A numerical value for number of cells or percentage (with statistics) is provided.

Methodology

Sample preparation	Cortex from BAC-GLT1-eGFP/8.3 kb-tdTomato double transgenic reporter mice (age P60-P90, n = 3 male mice per experiment) were analyzed with FACS. Mice were anesthetized with an intraperitoneal injection of ketamine xylazine. Brain tissue was immediately dissected and dissociated as previously described 16. Single cells were then sorted using a MoFlo MLS high-speed cell sorter and gated based on eGFP and tdTomato fluorescence.
Instrument	MoFlo MLS high speed cell sorter
Software	After hybridization, hybridization signals were acquired and normalized using Partek Genomics Suite software (Partek). Differential gene expression between conditions was assessed by statistical linear model analysis using Partek, Tibco Spotfire, and Prism 7 (GraphPad) software. The moderated t-statistic p-values derived from the Partek analysis above were further adjusted for multiple testing by Benjamini and Hochberg's method to control false discovery rate (FDR). An FDR cutoff of < 10% was used to obtain the list of differentially expressed genes.
Cell population abundance	A minimum of 100,000 cells were obtained per isolated cell population.
Gating strategy	Gating parameters are shown in the supplemental figures. Briefly, we validated proper gating of different cell populations by placing an allotted amount of cells on slides and imaged for corresponding fluorescence and cell specific markers. The Johns Hopkins FACS core was used.

☒ Tick this box to confirm that a figure exemplifying the gating strategy is provided in the Supplementary Information.